QED tests in magnetic fields

Prof. Carlo RIZZO,

Faculty of Science, University of Toulouse, Paul Sabatier

Laboratoire National des Champs Magnétiques Intenses (LNCMI)

Grenoble &Toulouse, France

outline

> **Magnetic fields**

- Vacuum QED
  - Vacuum magnetic birefringence
  - Non-linear electrodynamics

- Atoms : g-factors
  - Rubidium

High field magnets

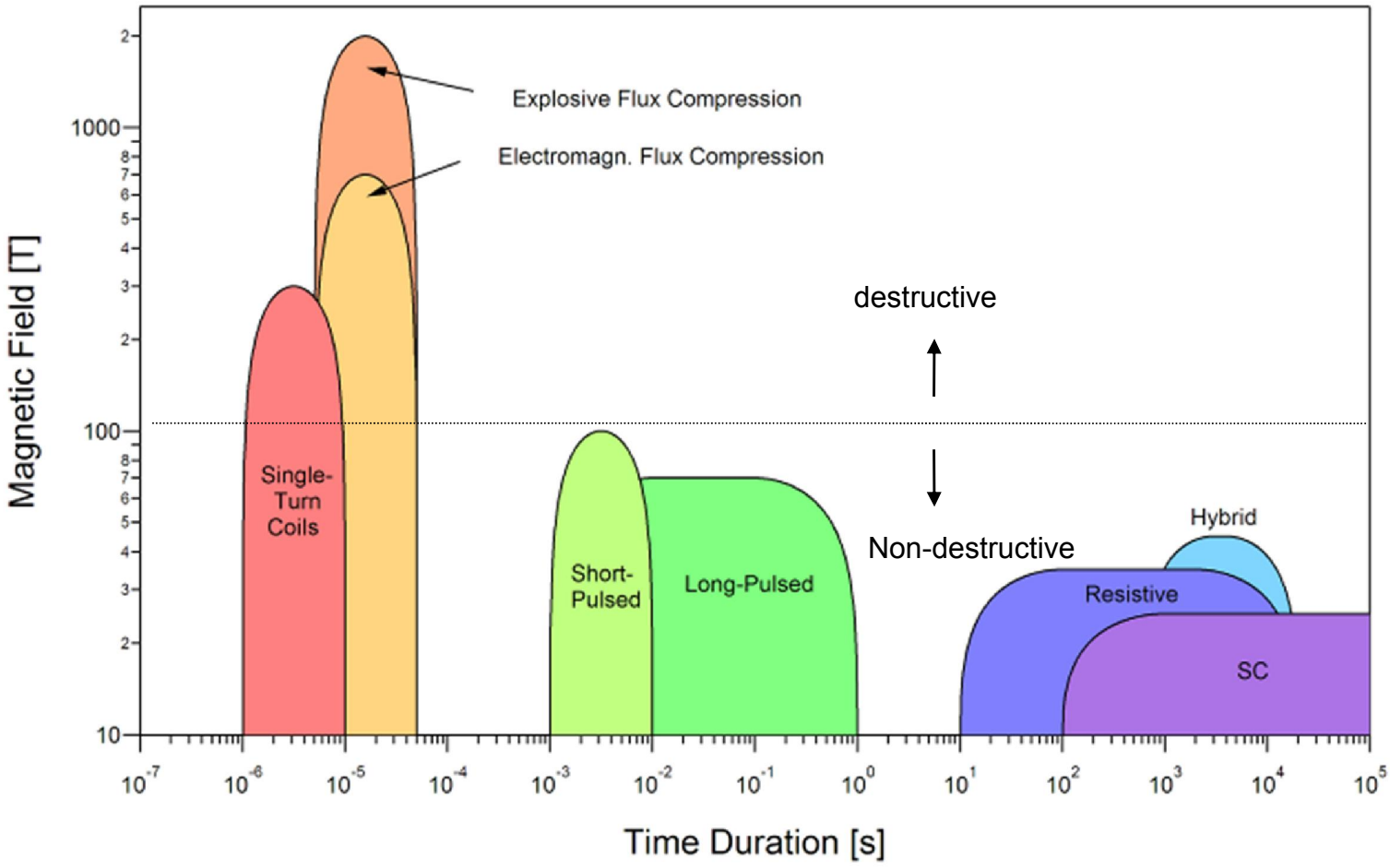

(semi)destructive pulsed static

Large high magnetic field facilities (pulsed and DC)

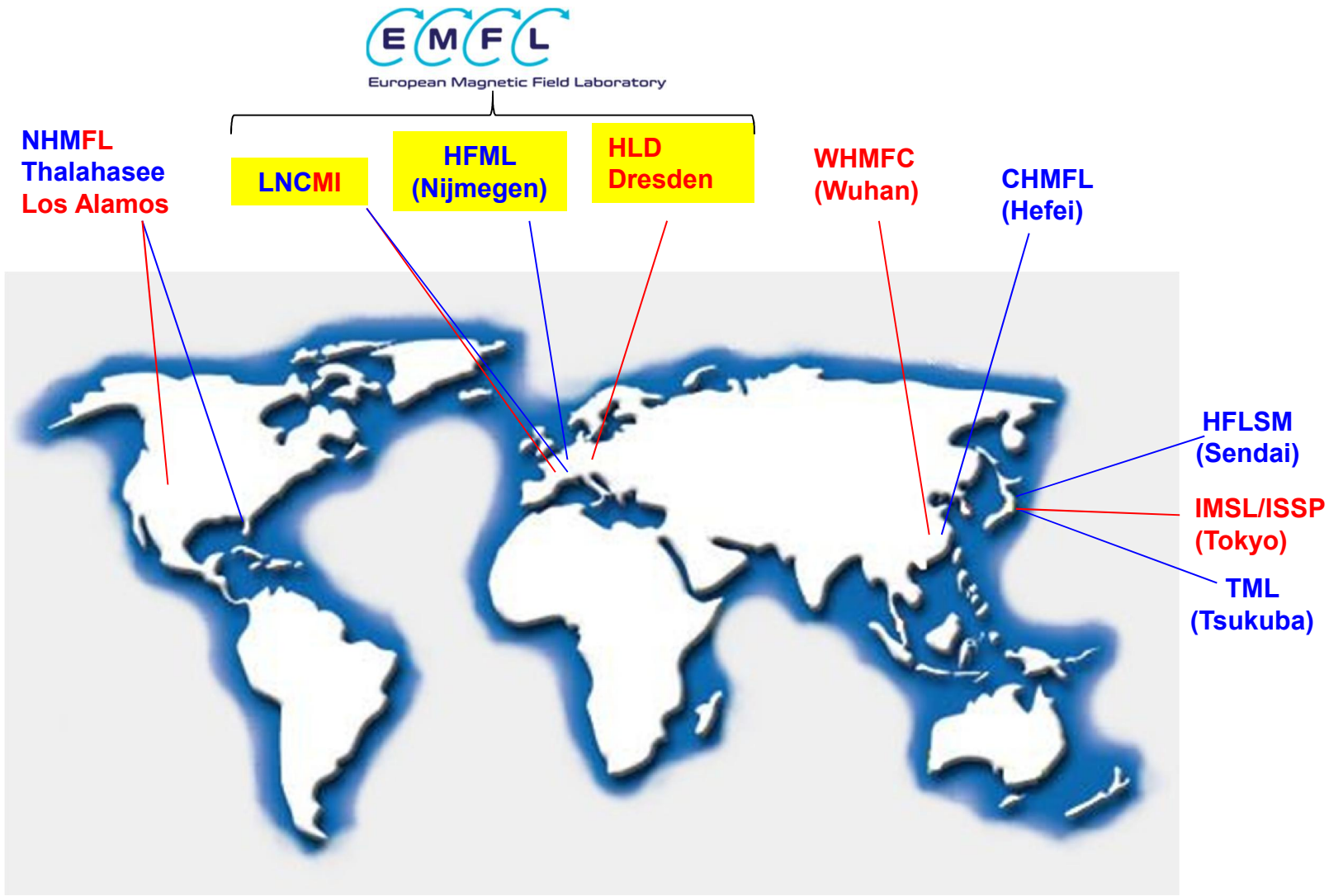

outline

> Magnetic fields

➢**Vacuum QED**
- ➢ Vacuum magnetic birefringence
- ➢ Non-linear electrodynamics

➢Atoms : g-factors
- ➢ Rubidium

Photon-photon interactions

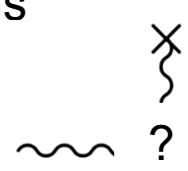

Classical vacuum

$$\nabla \times E = -\frac{\partial B}{\partial t},$$
$$\nabla \times H = \frac{\partial D}{\partial t},$$
$$\nabla \cdot D = 0,$$
$$\nabla \cdot B = 0,$$

$$H = \frac{1}{\mu_0} B - M,$$
$$D = \epsilon_0 E + P.$$

No interaction

QED vacuum

Heisenberg-Euler Lagrangian

$$F = \left(\epsilon_0 E^2 - \frac{B^2}{\mu_0}\right),$$
$$G = \sqrt{\frac{\epsilon_0}{\mu_0}}(E \cdot B).$$

$$P = 4c_{2,0}\epsilon_0 EF + 2c_{0,2}\sqrt{\frac{\epsilon_0}{\mu_0}}BG,$$
$$M = -4c_{2,0}\frac{B}{\mu_0}F + 2c_{0,2}\sqrt{\frac{\epsilon_0}{\mu_0}}EG.$$

$$c_{2,0} = \frac{2\alpha^2\hbar^3}{45m_e^4c^5} = \frac{\alpha}{90\pi}\frac{1}{\epsilon_0 E_{cr}^2}$$
$$= \frac{\alpha}{90\pi}\frac{\mu_0}{B_{cr}^2} \simeq 1.67 \times 10^{-30}\left[\frac{m^3}{J}\right],$$
$$c_{0,2} = 7c_{2,0},$$

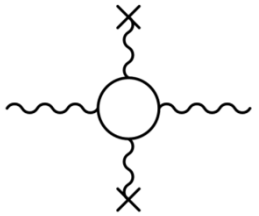

H. Euler and B. Kockel, Naturwissenschaften **23** 246 (1935)
W. Heinsenberg and H. Euler, Z. Phys. **38,** 714 (1936)

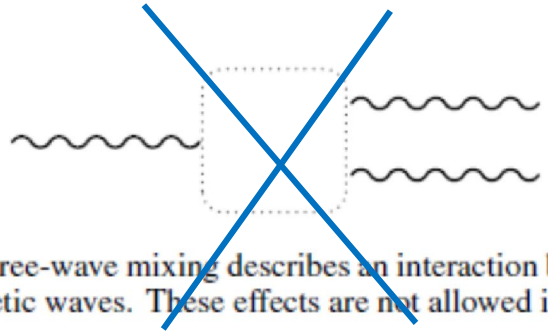

Figure 4. Three-wave mixing describes an interaction between three electromagnetic waves. These effects are not allowed in a vacuum.

Vacuum magneto-optics

Figure 5. Four-wave mixing. It represents the combination of four electromagnetic waves. These effects are allowed in vacuum.

DC effect

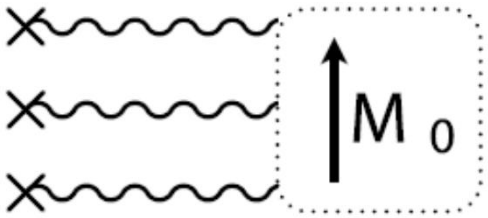

Figure 6. Four-wave mixing: three interactions of an electrostatic field give rise to a static magnetization.

see the review

R. Battesti, C. Rizzo, *Magnetic and electric properties of a quantum vacuum*, Rep. Prog. Phys. 76 (2013) 016401

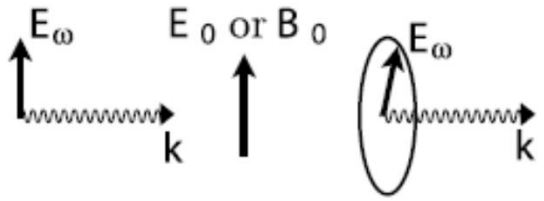

Figure 7. The Kerr effect or CME. A linear birefringence is induced by a static field (electric or magnetic) perpendicular to the direction of light propagation. A linear polarization is converted into an elliptical polarization thanks to the presence of a static field.

Light propagation

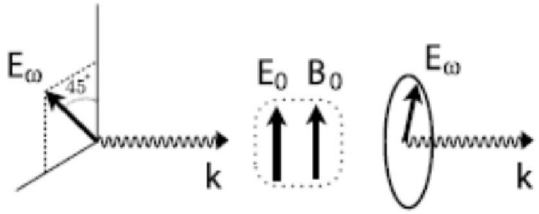

Figure 8. Jones linear birefringence. A linear birefringence is induced by both electric and magnetic fields perpendicular to the direction of light propagation. The birefringence axis is at ±45° with respect to the static fields.

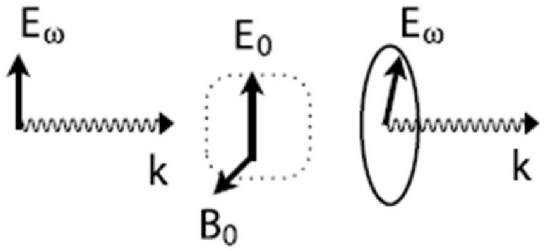

Figure 9. Magneto-electric linear birefringence. A linear birefringence is induced by crossed electric and magnetic fields, both perpendicular to the direction of light propagation. If one of the static fields is parallel to the direction of light propagation, the magneto-electric birefringence vanishes. One only obtains a birefringence due to the field being perpendicular to the direction of light propagation.

$$\Delta n_{\mathrm{CM}} = \left(\frac{2\alpha^2\hbar^3}{15m_e^4c^5} + \frac{5}{6}\frac{\alpha^3\hbar^3}{\pi m_e^4 c^5}\right)\frac{B_0^2}{\mu_0}$$
$$= \frac{2\alpha^2\hbar^3}{15m_e^4c^5}\left(1 + \frac{25\alpha}{4\pi}\right)\frac{B_0^2}{\mu_0}.$$

Vacuum birefringences

$$\Delta n_{\mathrm{K}} = -\frac{2\alpha^2\hbar^3}{15m_e^4c^5}\left(1 + \frac{25\alpha}{4\pi}\right)\epsilon_0 E_0^2,$$

$$\Delta n_{\mathrm{ME}} = -\frac{4\alpha^2\hbar^3}{15m_e^4c^5}\left(1 + \frac{25\alpha}{4\pi}\right)\sqrt{\frac{\epsilon_0}{\mu_0}}\frac{k}{k}\cdot(E_0 \times B_0),$$

$$\Delta n_{\mathrm{a}} = n(k) - n(-k) = -\frac{8\alpha^2\hbar^3}{15m_e^4c^5}\left(1 + \frac{25\alpha}{4\pi}\right)\sqrt{\frac{\epsilon_0}{\mu_0}}(E_0 B_0),$$

Static fields

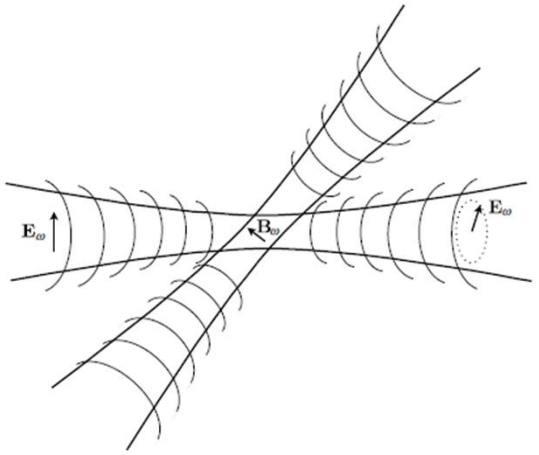

Figure 14. Optical field-induced birefringence. The external electric or magnetic field is produced by an electromagnetic wave. In this kind of experiment, a linearly polarized beam becomes elliptically polarized passing through another electromagnetic wave.

Laser fields

Figure 16. Parametric amplification induced by an electromagnetic field: splitting of a photon into two photons in the presence of a magnetic field.

Photon splitting
&
Photon fusion

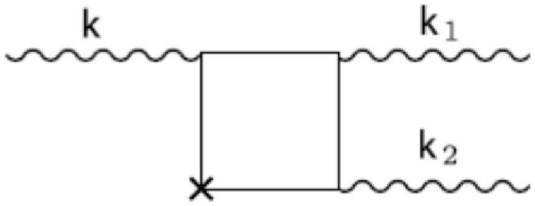

Figure 17. Box diagram for photon splitting with pump, signal and idler waves all collinear. The × denotes an interaction with the external field. The contribution of this diagram vanishes in a vacuum.

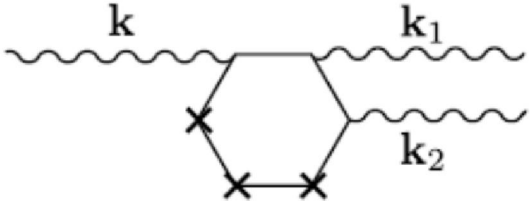

Figure 18. Hexagon diagram for photon splitting. Each × denotes an interaction with the external field.

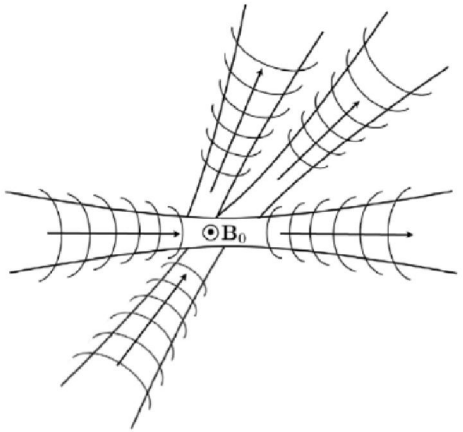

Figure 20. Optical field-induced photon splitting: photon splitting is induced by an electromagnetic field generated by an intense electromagnetic wave.

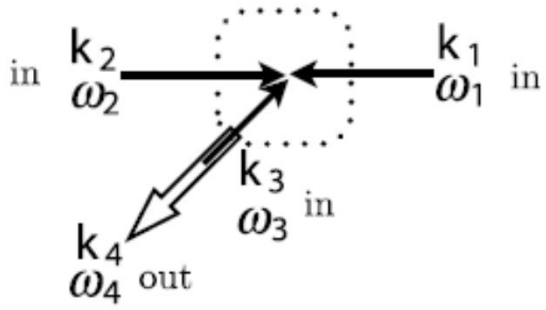

Figure 21. Photon–photon scattering in four wave mixing configuration. The collision of three beams satisfying the resonance condition in a vacuum $k_1 + k_2 = k_3 + k_4$ and $\omega_1 + \omega_2 = \omega_3 + \omega_4$ generate a fourth beam in the direction given by the matching conditions. The generated beam is stimulated by the third beam. This configuration avoids the detection of scattered incoming photons from the other beams.

Photon-Photon scattering

Already in the original paper of Euler-Kockel

Experimental tests in 2000 …

Bernard D, Moulin F, Amiranoff F, Braun A, Chambaret J P, Darpentigny G, Grillon G, Ranc S and Perrone F 2000 *Eur. Phys. J.* D **10** 141

Not observed

PHYSICAL REVIEW D **92,** 071301(R) (2015)

Vacuum birefringence in strong inhomogeneous electromagnetic fields

Felix Karbstein,[1,2] Holger Gies,[1,2] Maria Reuter,[1,3] and Matt Zepf[1,3,4]
[1]*Helmholtz-Institut Jena, Fröbelstieg 3, 07743 Jena, Germany*
[2]*Theoretisch-Physikalisches Institut, Abbe Center of Photonics, Friedrich-Schiller-Universität Jena, Max-Wien-Platz 1, 07743 Jena, Germany*
[3]*Institut für Optik und Quantenelektronik, Max-Wien-Platz 1, 07743 Jena, Germany*
[4]*Centre for Plasma Physics, School of Mathematics and Physics, Queen's University Belfast, Belfast BT7 1NN, United Kingdom*
(Received 8 July 2015; revised manuscript received 24 August 2015; published 26 October 2015)

Birefringence is one of the fascinating properties of the vacuum of quantum electrodynamics (QED) in strong electromagnetic fields. The scattering of linearly polarized incident probe photons into a perpendicularly polarized mode provides a distinct signature of the optical activity of the quantum vacuum and thus offers an excellent opportunity for a precision test of nonlinear QED. Precision tests require accurate predictions and thus a theoretical framework that is capable of taking the detailed experimental geometry into account. We derive analytical solutions for vacuum birefringence which include the spatio-temporal field structure of a strong optical pump laser field and an x-ray probe. We show that the angular distribution of the scattered photons depends strongly on the interaction geometry and find that scattering of the perpendicularly polarized scattered photons out of the cone of the incident probe x-ray beam is the key to making the phenomenon experimentally accessible with the current generation of FEL/high-field laser facilities.

Many experimental proposals :
Here one of the most recent.

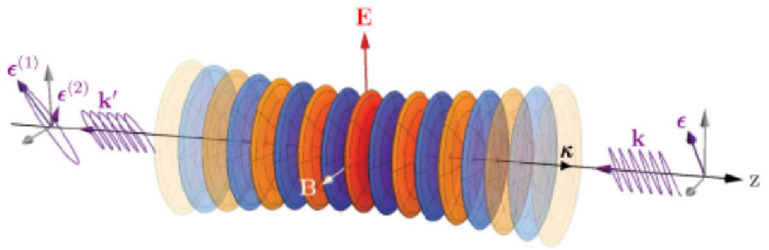

FIG. 1 (color online). Sketch of the pump-probe type scenario intended to verify vacuum birefringence. A linearly polarized optical high-intensity laser pulse—wavevector $\boldsymbol{\kappa}$, electric (magnetic) field **E** (**B**)—propagates along the positive z axis. Its strong electromagnetic field couples to the charged particle-antiparticle fluctuations in the quantum vacuum, and thereby effectively modifies its properties to be probed by a counter-propagating x-ray beam (wavevector **k**, polarization $\boldsymbol{\epsilon}$). Vacuum birefringence manifests itself in an ellipticity of the outgoing x-ray photons (wavevector **k′**, polarization components along $\boldsymbol{\epsilon}^{(1)}$ and $\boldsymbol{\epsilon}^{(2)}$).

see the review
R. Battesti, C. Rizzo, *Magnetic and electric properties of a quantum vacuum*, Rep. Prog. Phys. 76 (2013) 016401

outline

> Magnetic fields

- Vacuum QED
  - **Vacuum magnetic birefringence**
  - Non-linear electrodynamics

- Atoms : g-factors
  - Rubidium

VMB at the LNCMI : the BMV project

Grenoble, France

DC fields

36 T / 43 T in project

Toulouse, France

Pulsed fields

91 T 10 ms

❑ Vacuum magnetic birefringence (VMB)

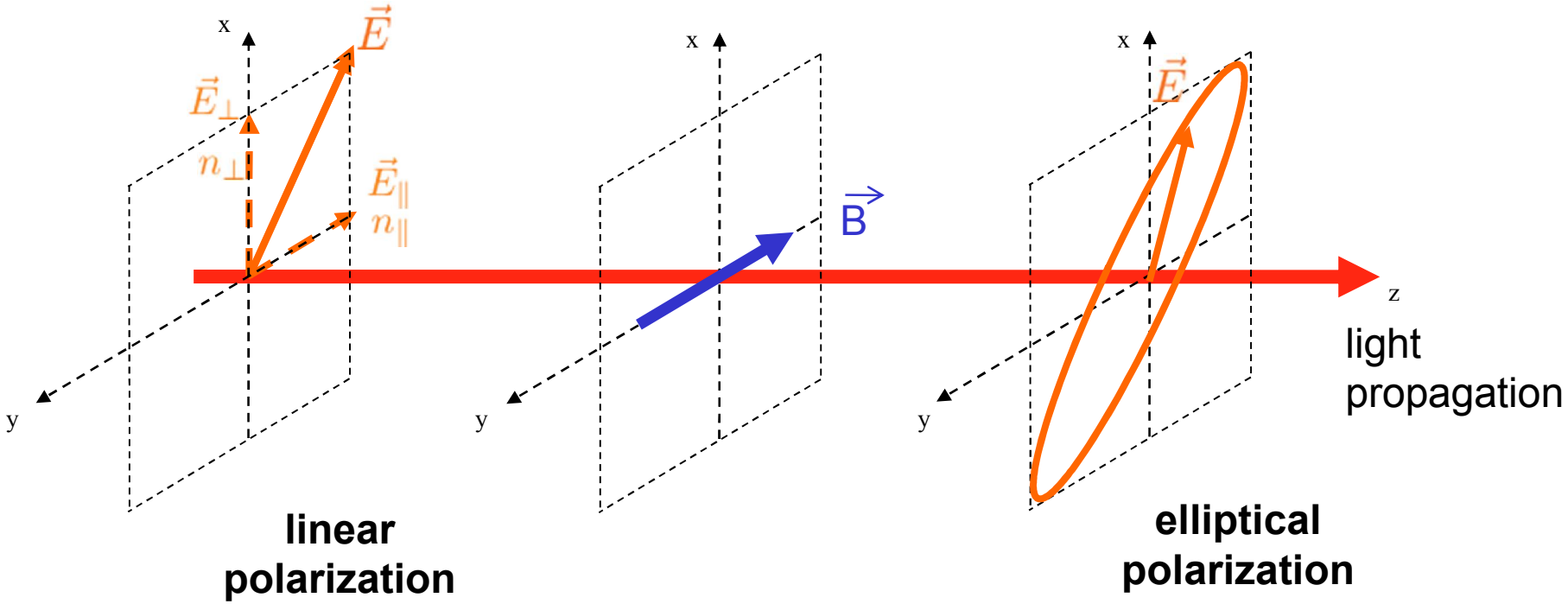

This effect exists in **any** medium, even in **vacuum**

Effect as old as 1935,

but still not observed

H. Euler and B. Kockel, Naturwissenschaften **23** 246 (1935)

W. Heinsenberg and H. Euler, Z. Phys. **38,** 714 (1936)

❑ Vacuum magnetic birefringence

$$\Delta n = \left(\frac{2\alpha^2\hbar^3}{15 m_e^4 c^5} + \frac{5}{6}\frac{\alpha^3\hbar^3}{\pi m_e^4 c^5} \right) \frac{B_0^2}{\mu_0} = \frac{2\alpha^2\hbar^3}{15 m_e^4 c^5} \left(1 + \frac{25\alpha}{4\pi} \right) \frac{B_0^2}{\mu_0}$$

$$\Delta n = k_{CM}\ B^2$$

CODATA 2012

$$k_{CM} = (4.0317 \pm 0.0009) \times 10^{-24}\ \mathrm{T}^{-2}$$

a very challenging task !

Z. Bialynika-Birula et al., Phys. Rev. D **2,** 2341 (1970)

❑ Ellipticity measurement

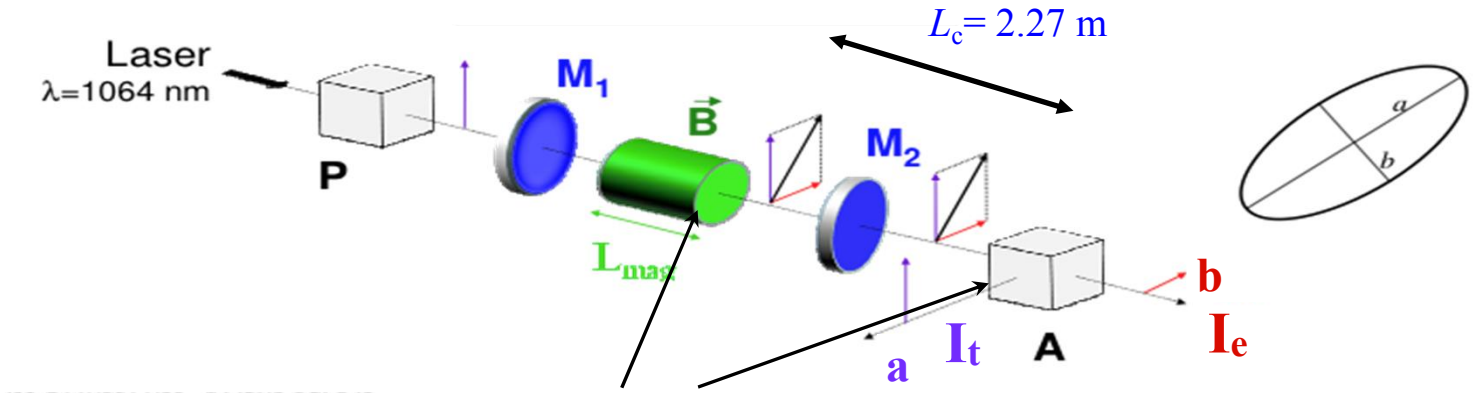

Fabry Perot cavity

Very high magnetic field
+
Very precise optical measurements

• Ellipticity to be measured :

$$\Psi(t) = \frac{\pi}{\lambda} k_{CM} \left(\frac{2F}{\pi}\right) B(t)^2 L_{mag} \sin(2\theta_p)$$

$$F \simeq 450\ 000$$ → light trapped for ~ 300 Km in the magnetic field !

Cotton-Mouton effect of Helium

P = 450x10^{-3} atm

Experimental data

fit αB^2

$\alpha \sim 2 \times 10^{-16}\ T^{-2}\ atm^{-1}$

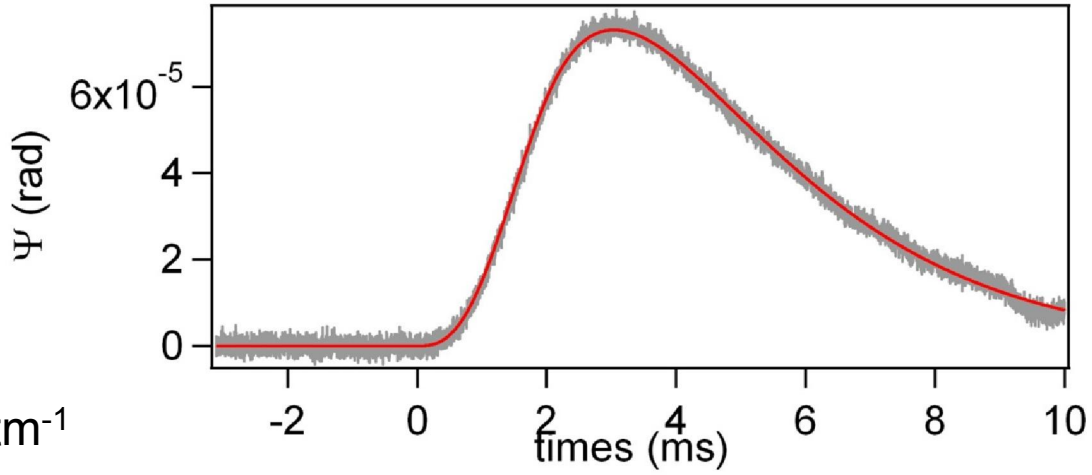

Vacuum zero signal

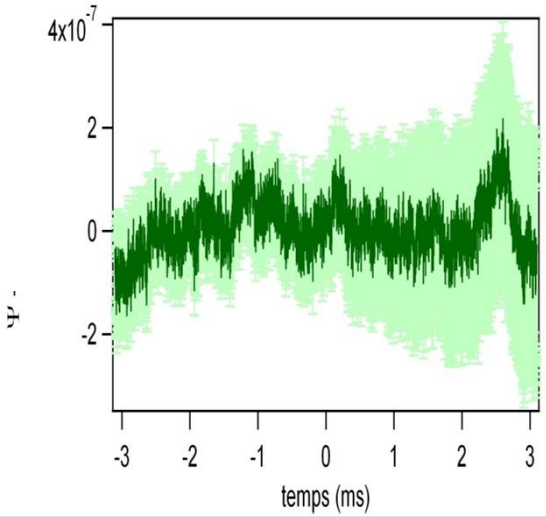

$$k_{CM} = (8.3 \pm 8.0) \times 10^{-21}\ \mathrm{T}^{-2}$$

A. Cadène *et al*,

Eur. Phys. J. D, **68**, 16 (2014)

$$k_{CM} = (8.3 \pm 8.0) \times 10^{-21}\ \mathrm{T}^{-2}$$

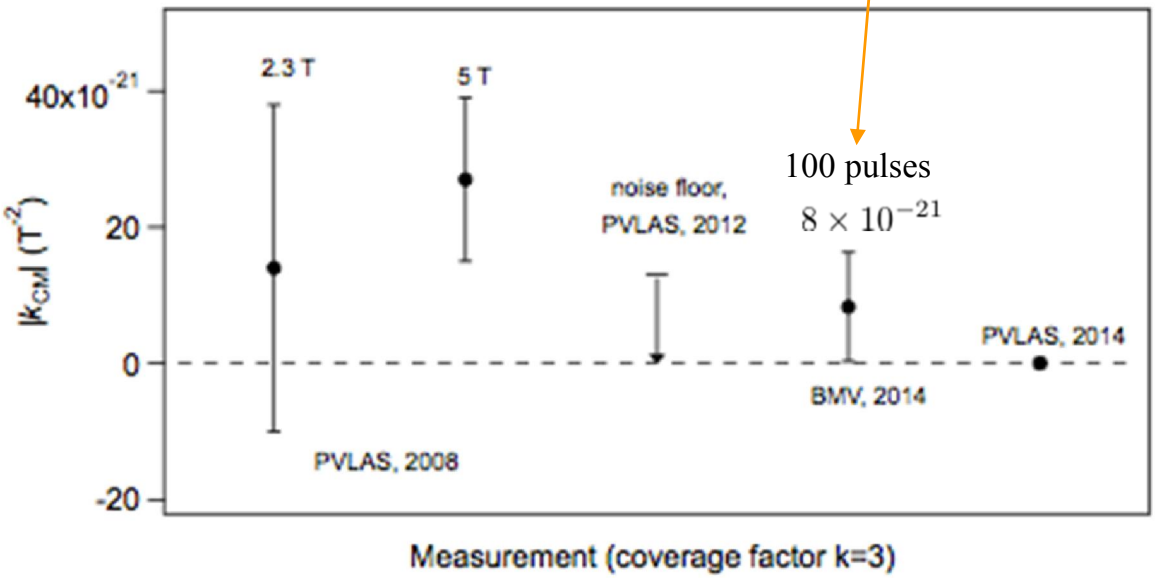

The race for the VMB in vacuum

recent results :
PVLAS is heading again !
A factor 50 from goal !

PVLAS, 2008: E. Zavattini *et al*., *Phys. Rev. D* **77**, 032006 (2008)

PVLAS, 2012: G. Zavattini *et al*., *Int. J. of Mod. Phys. A* **27**, 1260017 (2012)

BMV 2014 : A. Cadène *et al*, Eur. Phys. J. D, **68**, 16 (2014)

PVLAS 2014 : F. Della Valle et al, *Phys. Rev. D* **90**, 092003 (2014)

+ Q&A Taiwan
+ OSQAR CERN
+ Very intense laser sources …

- signal enhancement

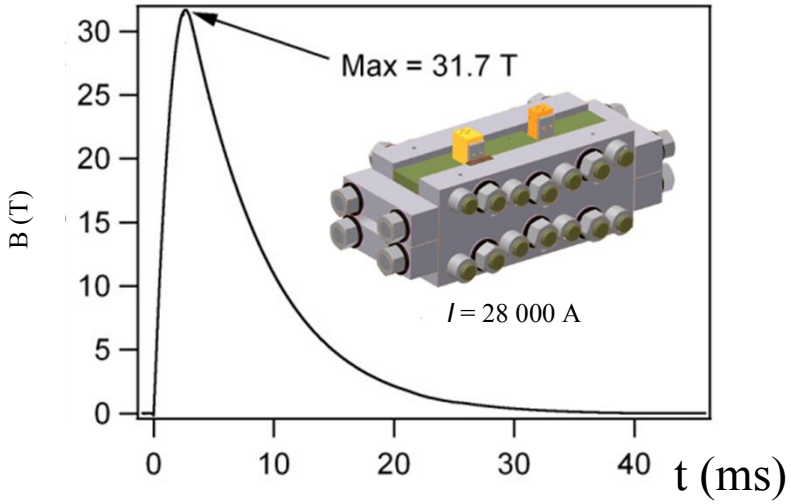

Magnetic field : (2 XXL-Coils)

- Higher B^2L ($300\ T^2m$)

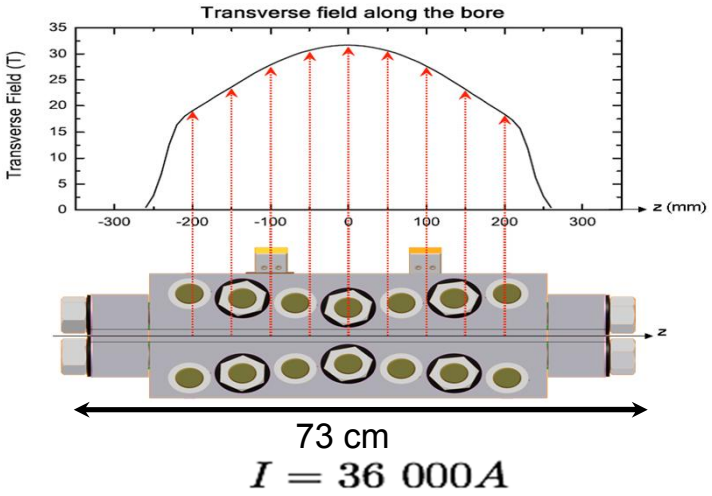

Cavity mirrors :

- Higher finesse (goal : 1 million). Partnership with the LMA of Villeurbanne, France (also producing mirrors for VIRGO & LIGO)

❑ noise and spurious signal reduction

- ❑ Better polarizer extinction ratio
- ❑ Acoustic noise attenuation

3D drawing

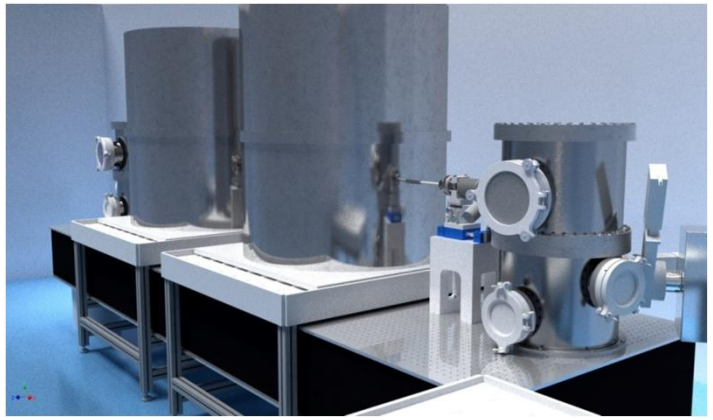

- ❑ More stable Laser locking to the cavity
- ❑ Magnetic field shielding

Current status

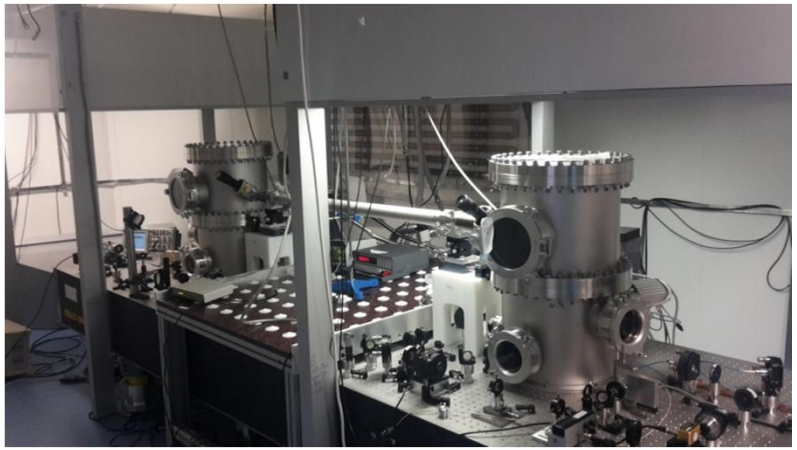

- ❑ Data acquisition procedure (B at 0° and 45° with respect to the polarization)

outline

> Magnetic fields

- Vacuum QED
  - Vacuum magnetic birefringence
  - **Non-linear electrodynamics**
- Atoms : g-factors
  - Rubidium

This is nice, but what's for ? QED is very well tested !

Non-Linear Electrodynamics

$$\mathcal{L} = \sum_{i=0}^{\infty}\sum_{j=0}^{\infty} c_{i,j}\mathcal{F}^i\mathcal{G}^j.$$

The number of free parameters $c_{i,j}$ is infinite,

$$\begin{aligned}
\mathcal{L} &= \mathcal{L}_0 + \mathcal{L}_{\rm NL} \\
\text{with}\quad \mathcal{L}_0 &= \frac{1}{2}\mathcal{F} \\
\text{and}\quad \mathcal{L}_{\rm NL} &\simeq c_{0,1}\mathcal{G} + c_{2,0}\mathcal{F}^2 + c_{0,2}\mathcal{G}^2 + c_{1,1}\mathcal{F}\mathcal{G}.
\end{aligned}$$

$$\begin{aligned}
\mathbf{P} &= c_{0,1}\sqrt{\frac{\epsilon_0}{\mu_0}}\mathbf{B} \\
&+ 4c_{2,0}\epsilon_0\mathcal{F}\mathbf{E} \\
&+ 2c_{0,2}\sqrt{\frac{\epsilon_0}{\mu_0}}\mathcal{G}\mathbf{B} \\
&+ c_{1,1}\left(2\epsilon_0\mathcal{G}\mathbf{E} + \sqrt{\frac{\epsilon_0}{\mu_0}}\mathcal{F}\mathbf{B}\right), \\
\mathbf{M} &= c_{0,1}\sqrt{\frac{\epsilon_0}{\mu_0}}\mathbf{E} \\
&- 4c_{2,0}\mathcal{F}\frac{\mathbf{B}}{\mu_0} \\
&+ 2c_{0,2}\sqrt{\frac{\epsilon_0}{\mu_0}}\mathcal{G}\mathbf{E} \\
&- c_{1,1}\left(2\mathcal{G}\frac{\mathbf{B}}{\mu_0} - \sqrt{\frac{\epsilon_0}{\mu_0}}\mathcal{F}\mathbf{E}\right).
\end{aligned}$$

see
M. Fouché, R. Battesti, C. Rizzo, *Limits on non-linear electrodynamics*, arXiv:1605.04102 in press PRD

Heisenberg and Euler effective lagrangian

$$\mathcal{L}_{\rm NL} = \frac{\alpha}{90\pi}\frac{1}{\epsilon_0 E_{cr}^2}[\mathcal{F}^2 + 7\mathcal{G}^2].$$

$$\begin{aligned} c_{1,0} &= \frac{1}{2}, \qquad c_{0,1} = 0 \text{ and } c_{1,1} = 0 \\ c_{2,0} &= \frac{2\alpha^2\hbar^3}{45 m_e^4 c^5} \qquad c_{0,2} = 7c_{2,0}, \\ &= \frac{\alpha}{90\pi}\frac{1}{\epsilon_0 E_{\rm cr}^2} = \frac{\alpha}{90\pi}\frac{\mu_0}{B_{\rm cr}^2} \end{aligned}$$

Born-Infeld effective lagrangian

$$\mathcal{L} \simeq \frac{1}{2}\mathcal{F} + \frac{1}{8\epsilon_0 E_{\rm abs}^2}\mathcal{F}^2 + \frac{1}{2\epsilon_0 E_{\rm abs}^2}\mathcal{G}^2.$$

$$\begin{aligned} c_{1,0} &= \frac{1}{2}, \\ c_{0,1} &= c_{1,1} = 0, \\ c_{2,0} &= \frac{1}{8\epsilon_0 E_{\rm abs}^2}, \\ c_{0,2} &= \frac{1}{2\epsilon_0 E_{\rm abs}^2} = 4c_{2,0}. \end{aligned}$$

Lagrangian in the string theory framework

$$\mathcal{L} = \frac{1}{2}\mathcal{F} + \frac{\gamma}{4}\left[(1-b)\mathcal{F}^2 + 6\mathcal{G}^2\right]$$

$$\begin{aligned} c_{1,0} &= \frac{1}{2}, \\ c_{0,1} &= c_{1,1} = 0, \\ c_{2,0} &= \frac{\gamma}{4}(1-b), \\ c_{0,2} &= \frac{3}{2}\gamma. \end{aligned}$$

...

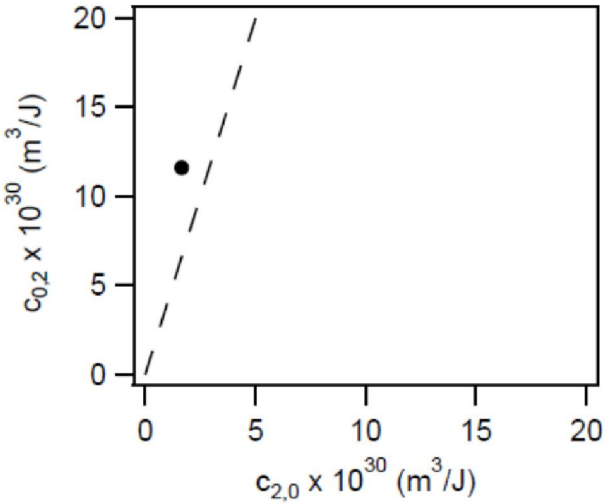

FIGURE 1: Born-Infeld prediction and Heisenberg-Euler prediction in the $(c_{2,0}, c_{0,2})$ parameter space. The Born-Infled prediction is represented by a straight line, while the Heisenberg-Euler one is a point.

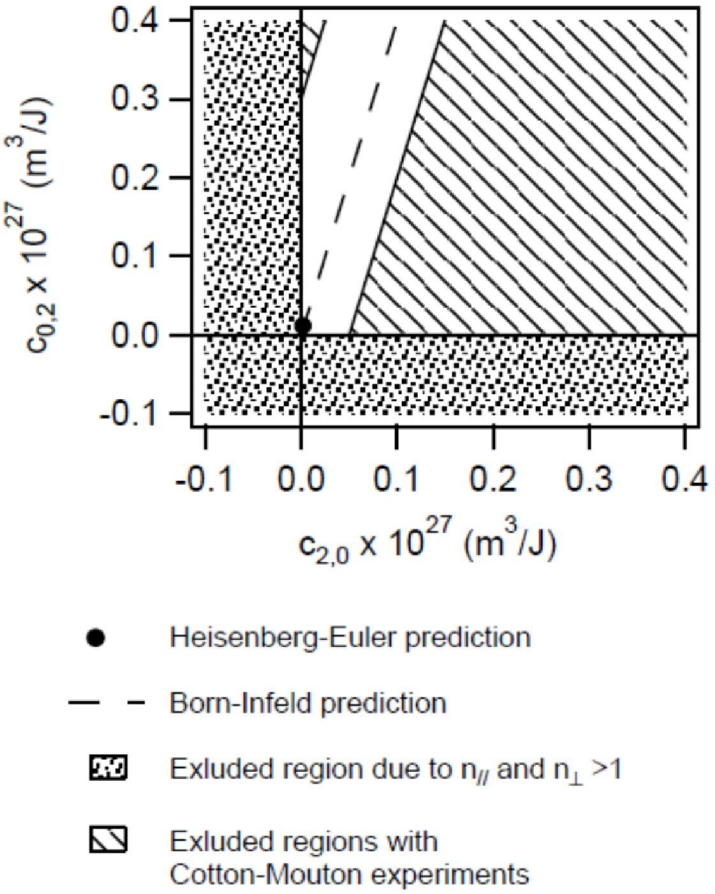

NLED prediction for a particle having a charge and a magnetic moment :

Wichmann-Kroll correction

$$\mathbf{E_V} = \mathbf{E}\left[1 - c_{2,0}\frac{Q^2}{4\pi^2\epsilon_0 r^4}\right]$$

System and energy levels	Wichmann-Kroll contribution to the leading term	Experimental relative uncertainty	Remarks
H 1S	0.3 ppm	3 ppm [45]	
H muonic 2S-2P	5 ppm	15 ppm [46]	Proton charge radius puzzle

TABLE II: Examples of the contribution of the Wichmann-Kroll correction to the Lamb shift leading term for two different energy transitions and systems, to be compared to the relative uncertainties obtained on the Lamb shift measurements [47].

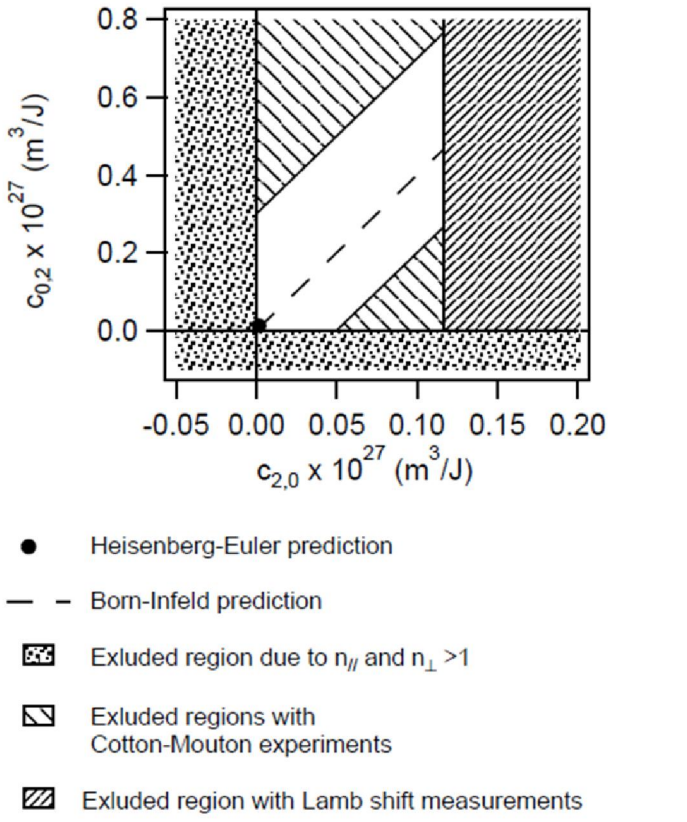

FIGURE 3: Best experimental limits on $c_{0,2}$ and $c_{2,0}$ parameters. The excluded region due to Lamb shift measurements is added.

Behond QED : Axionic particles that couples with two photons

Virtual particle

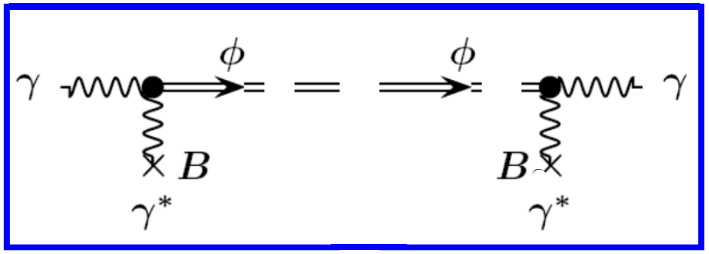

Ellipticity

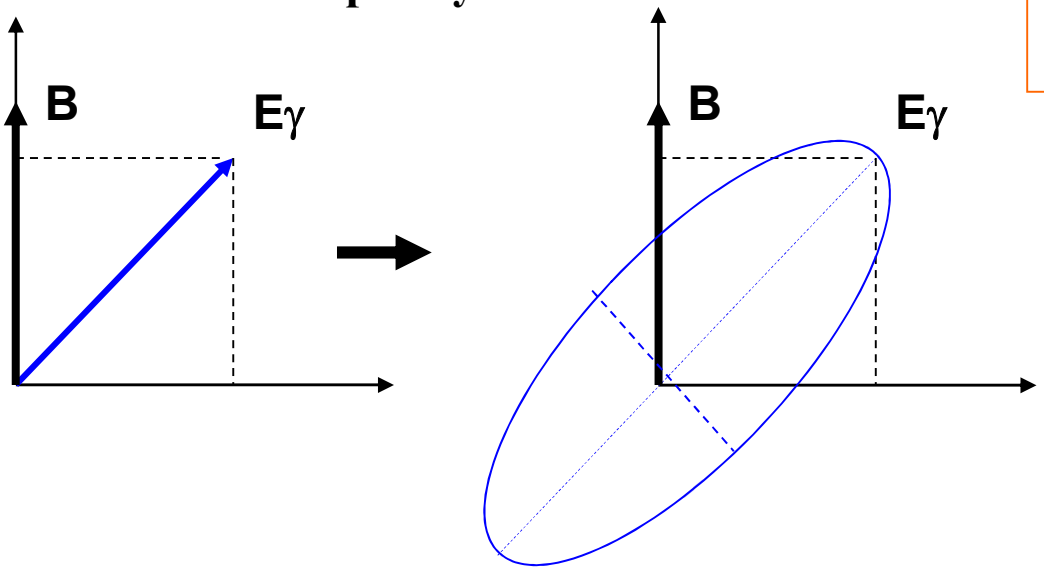

Δn > 0 ⇨ Pseudoscalar

Δn < 0 ⇨ Scalar

L.Maiani, R.Petronzio et E.Zavattini, *Phys. Lett. B* **175** (1986) 359

- Axion source and detection on earth :

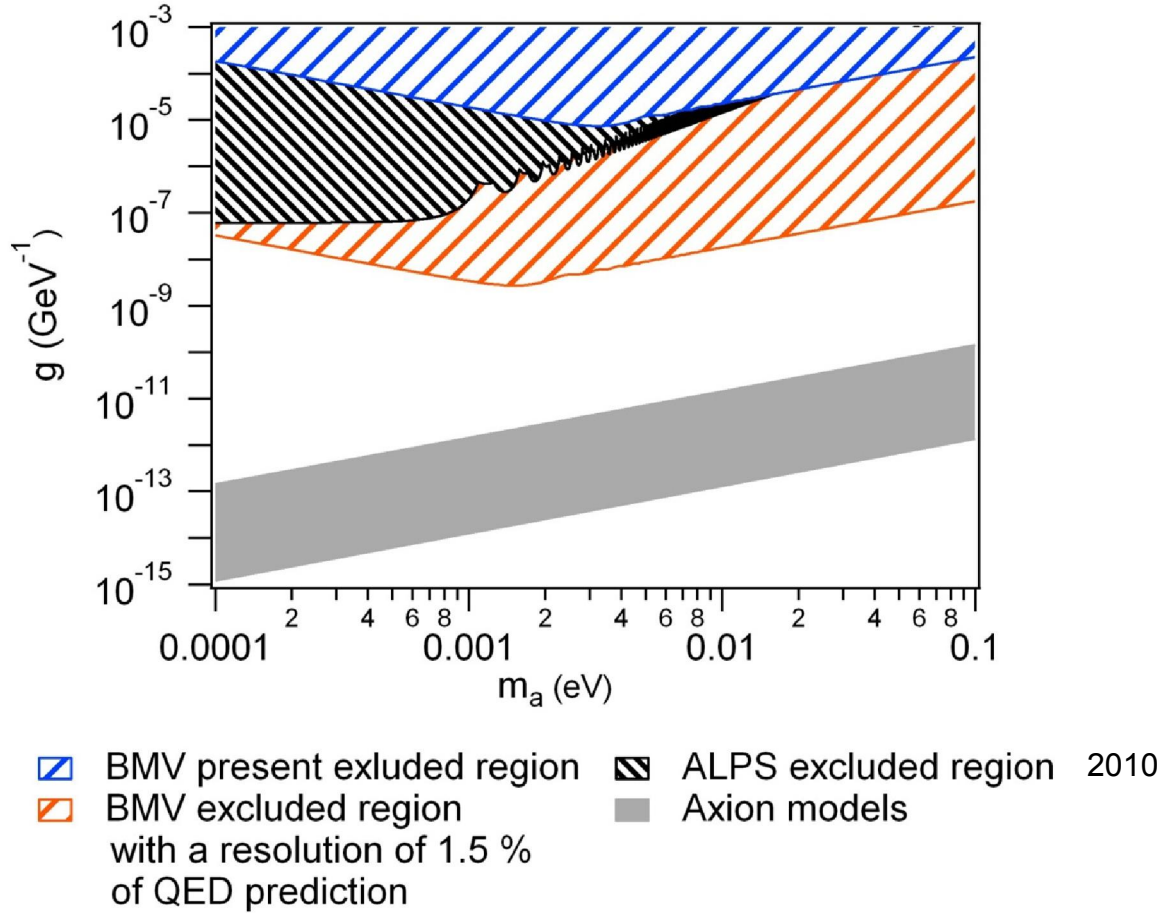

ALPS : K. Ehret et al., Phys. Lett. B **689**, 149 (2010)

outline

> Magnetic fields

- Vacuum QED
  - Vacuum magnetic birefringence
  - Non-linear electrodynamics

- **Atoms : g-factors**
  - Rubidium

outline

> Magnetic fields

- Vacuum QED
  - Vacuum magnetic birefringence
  - Non-linear electrodynamics

- **Atoms : g-factors**
  - Rubidium

How does one measure
a pulsed field accurately ?

Atom + Magnetic field : Zeeman interaction

$$\mathcal{H}_Z = -(\vec{\mu}_L + \vec{\mu}_S + \vec{\mu}_I) \cdot \vec{B} =$$
$$(g_L L_z + g_S S_z)\mu_B B - g_I I_z \mu_N B = (g_L L_z + g_e S_z + g'_I I_z)\mu_B B,$$

$g_J \boldsymbol{J}$

The Russel-Saunders coupling of the angular momenta predicts the following g_J value:

$$g_J = g_S \frac{J(J+1) + S(S+1) - L(L+1)}{2J(J+1)} + g_L \frac{J(J+1) - S(S+1) + L(L+1)}{2J(J+1)}.$$

$g_s = g_e \neq g$ of the free electron

Matter for QED theoreticians

Spectroscopy of Natural and Artificial Atoms in Magnetic Fields
Advances In Atomic, Molecular, and Optical Physics, *In Press,* E. Arimondo, D. Ciampini, C. Rizzo

outline

> Magnetic fields

- Vacuum QED
  - Vacuum magnetic birefringence
  - Non-linear electrodynamics

- Atoms : g-factors
  - **Rubidium**

RUbidium in High MAgnetic field :
RUHMA

Funded by NEXT

Collaboration between LNCMI BMV group
& BEC Group of Dep. of Physics,
University of Pisa, Italy
of Prof. E. Arimondo

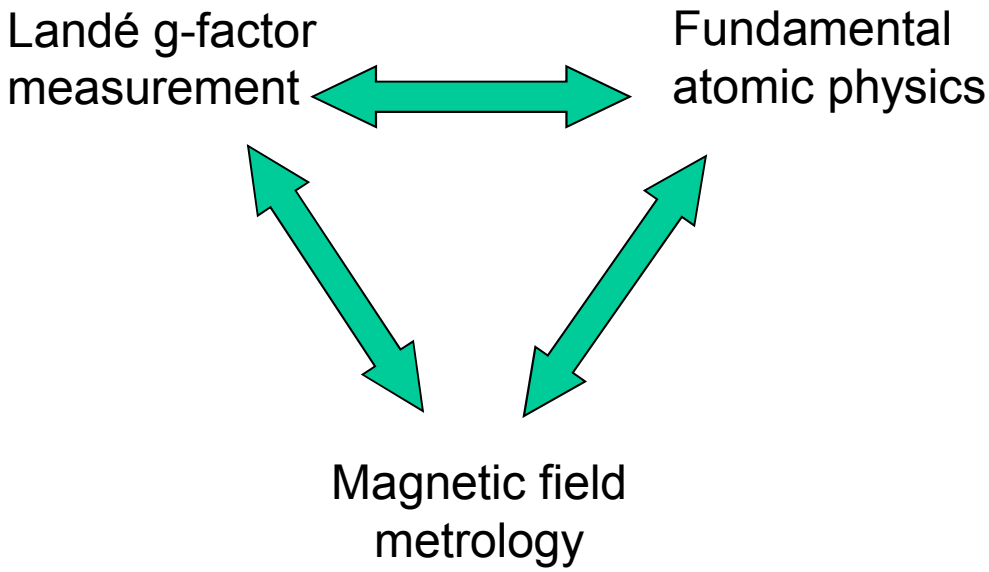

Rubidium atoms “D2” energy diagram

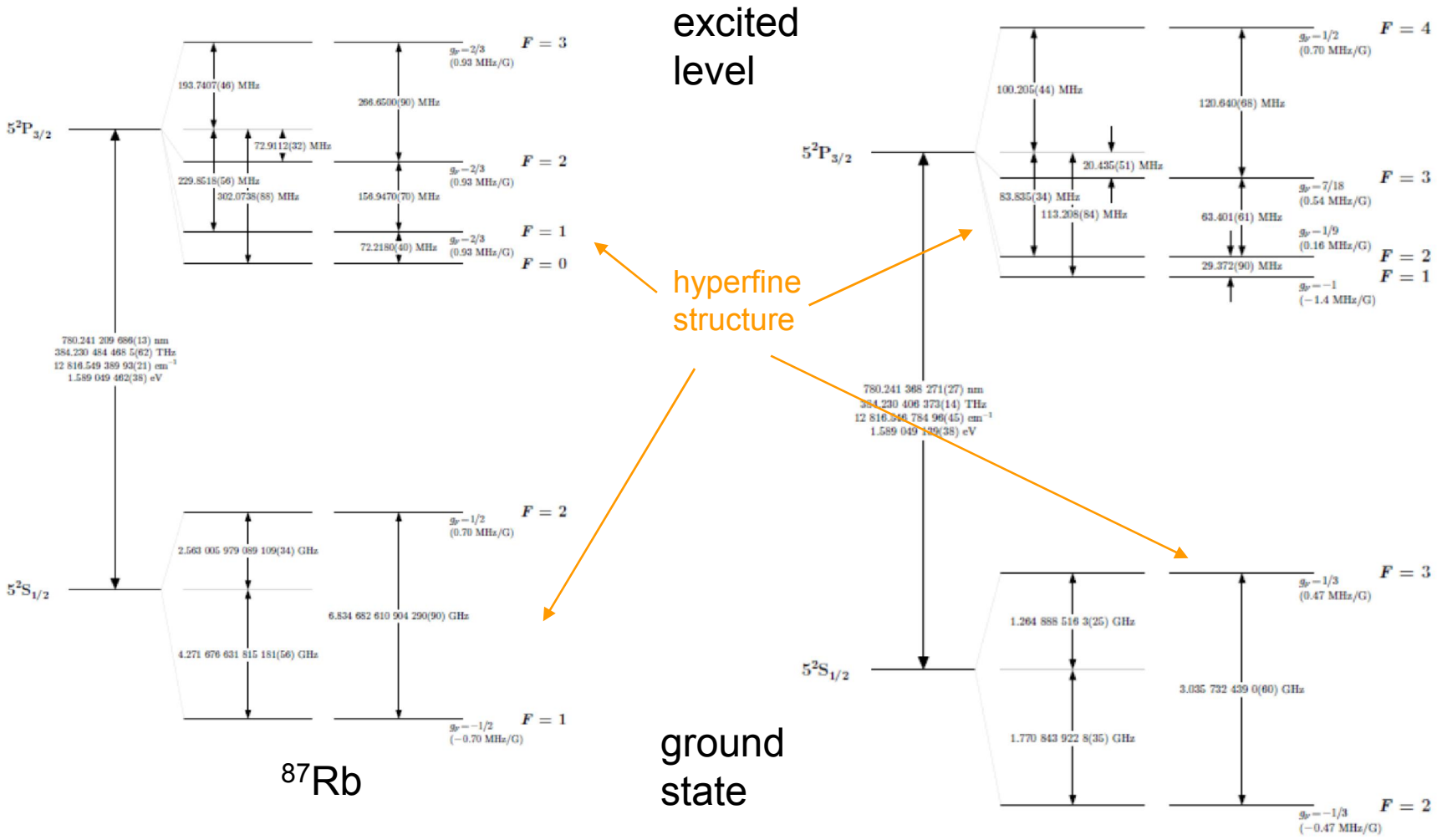

^{87}Rb

^{85}RB

transition frequency : 384.2304844685(62) THz
transition wavelength : 780.244209686(13) nm

g_j^g = 2.002331113(20) for the ground state
g_i^g = -0.0009951414(10)

Δg deviations from the free electron value for the g-factor in Rb excited states

Excited state	Δg_{exp}	Δg_{rel}
$5P_{1/2}$	not available	not available
$5P_{3/2}$	$2100(1300) \times 10^{-6}$ [4]	not available
$nD_{3/2}$	not available	-13×10^{-6}[6] for n=4
$nD_{5/2}$	-650(1500) [4] for n=8	-6×10^{-6}[6] for n=4

[4] E. Arimondo, M. Inguscio and P. Violino, Rev. Mod. Phys. **49**, 31 (1977).

[6] G. H. Gossel, V. A. Dzuba, and V. V. Flambaum, Phys. Rev. A **88**, 034501 (2013).

illustration of the experimental method

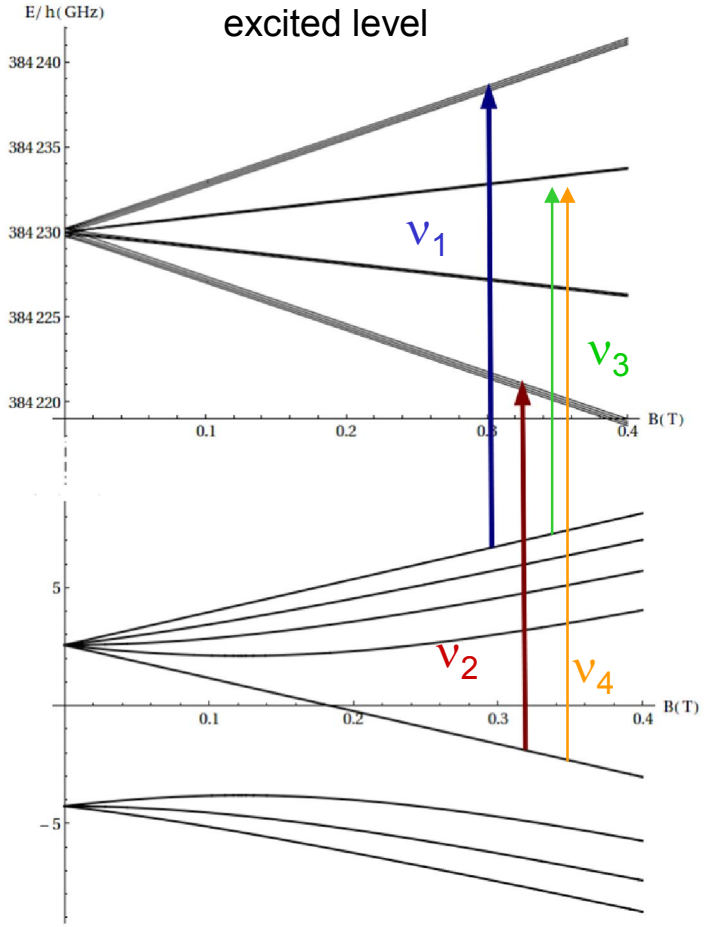

$5P_{3/2}$

Spectroscopy notation

$5S_{1/2}$

For an unknown value of B, one measures : ν_1, ν_2, ν_3, ν_4 ...

ν_3 ,ν_4 depend on
ν_1 ,ν_2 B and g_j^e
and to other known quantities

One can give both B and g_j^e

At the best of our knowledge,

the “signal” (frequency difference) grows with B ≈ 14 000 MHz/T

the “noise” (frequency measurement precision) do not depends on B

therefore “signal to noise ratio” increases with B

Precisions of 100 ppm on the above signal are necessary to improve existing data

14 MHz

0.14 MHz

at 10 T

Precisions of 1 ppm are necessary to test QED theory

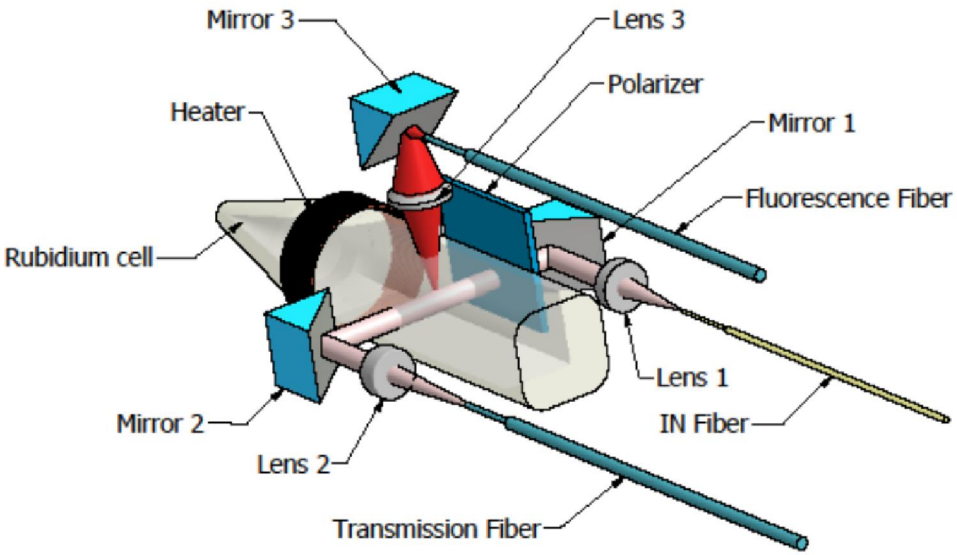

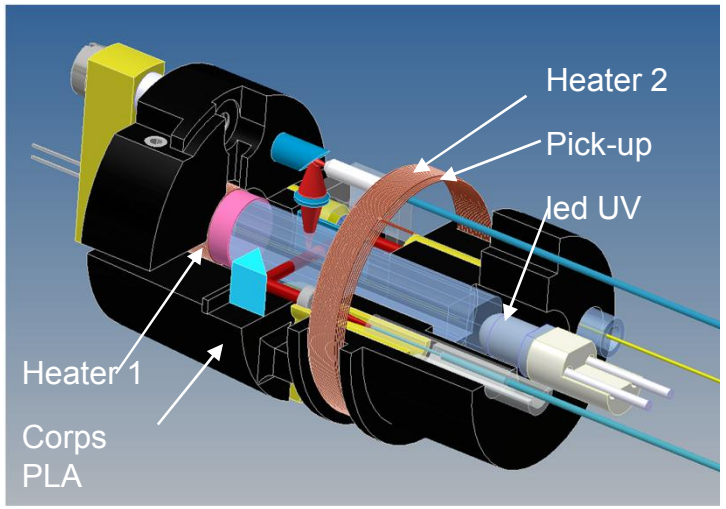

realized thanks to a 3D printer

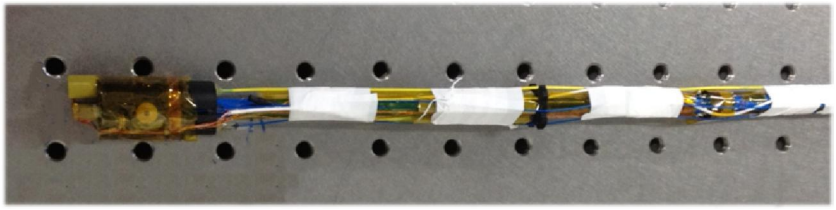

The complete probe

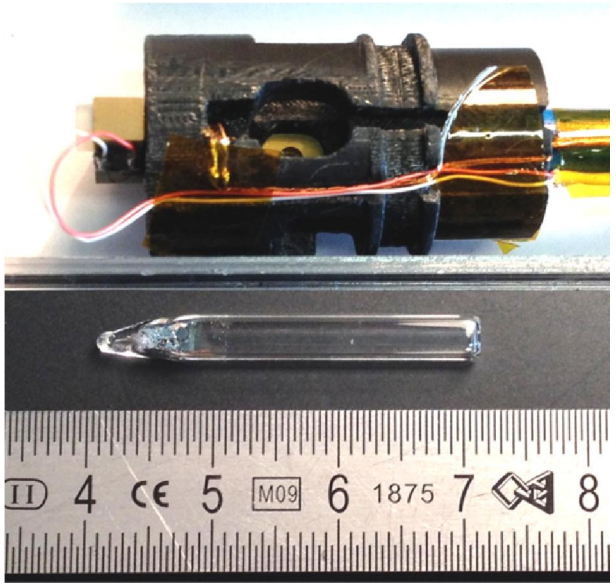

Laser frequency is fixed

One month ago data

Pulsed magnetic field

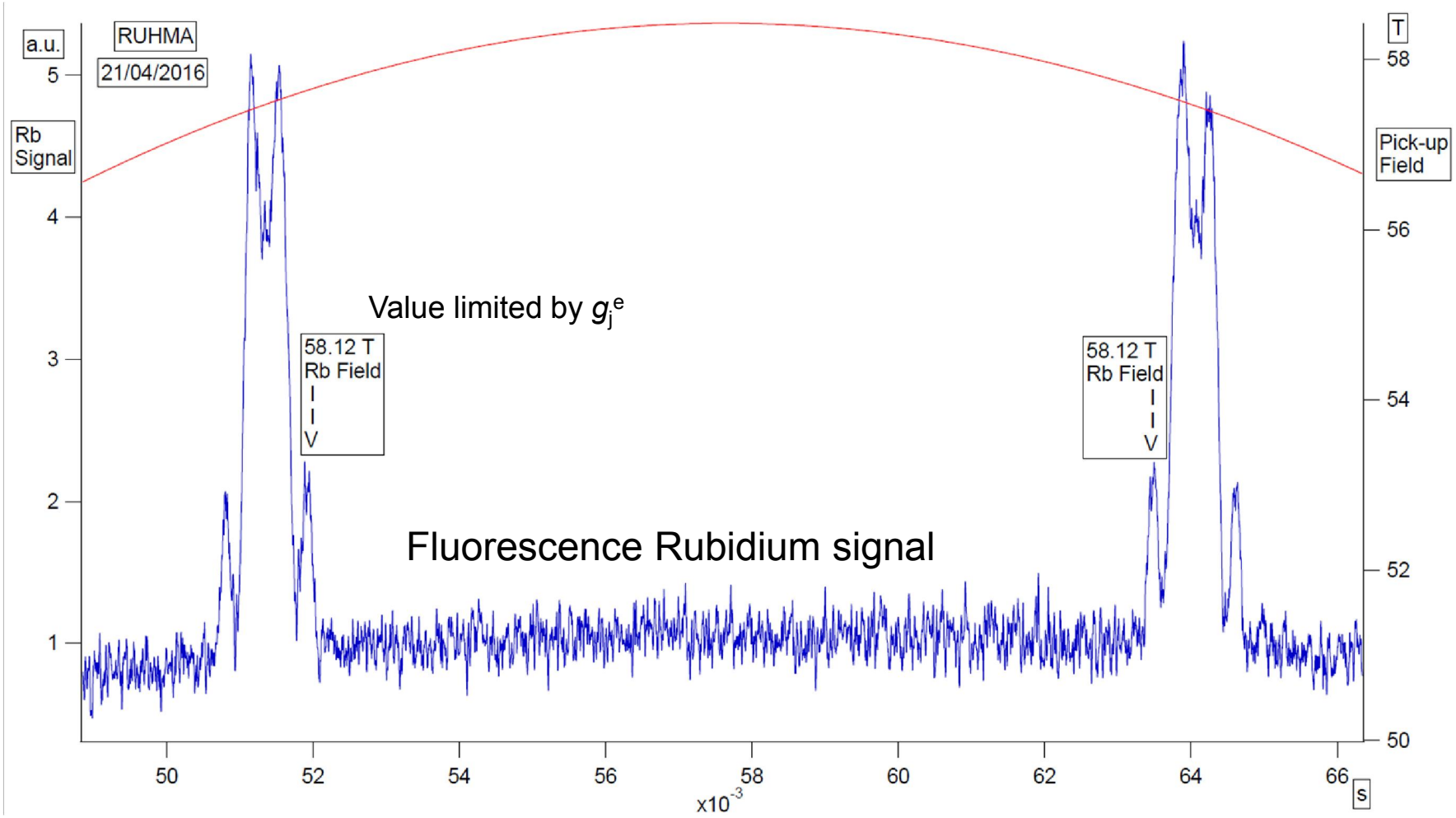

World record for a gas !

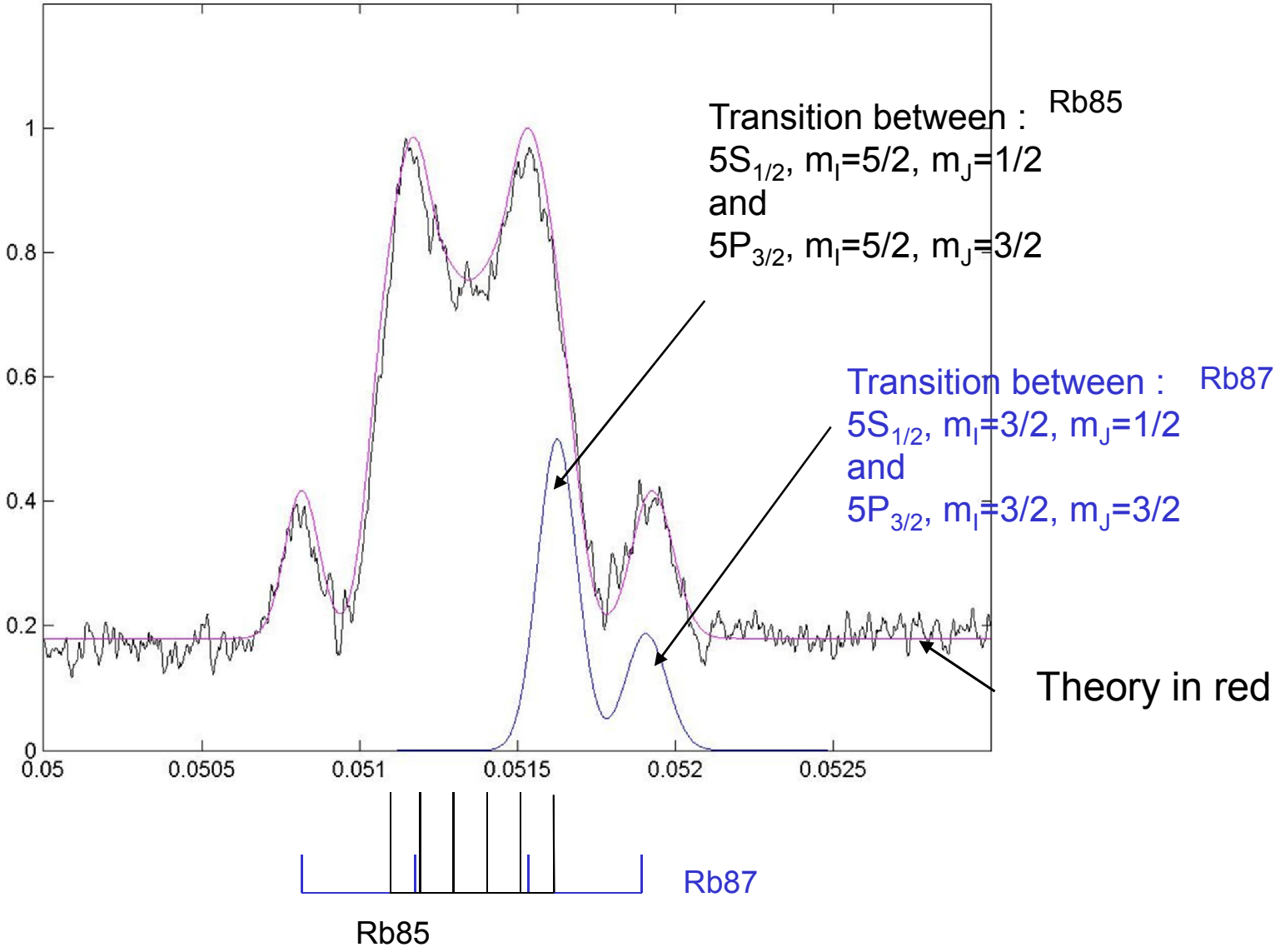
Transition between : Rb85
$5S_{1/2}$, m_I=5/2, m_J=1/2
and
$5P_{3/2}$, m_I=5/2, m_J=3/2
Transition between : Rb87
$5S_{1/2}$, m_I=3/2, m_J=1/2
and
$5P_{3/2}$, m_I=3/2, m_J=3/2
Theory in red
0
0.2
0.4
0.6
0.8
1
0.05
0.0505
0.051
0.0515
0.052
0.0525
Rb87
Rb85

Conclusion

New version of BMV will eventually observe the VMB effect
(hopefully we will arrive first)

RUHMA : first accurate measurement of the field done,
space now for g measurements and/or better accuracy …

QED tests in magnetic fields

Prof. Carlo RIZZO,

Faculty of Science, University of Toulouse, Paul Sabatier

Laboratoire National des Champs Magnétiques Intenses (LNCMI)

Grenoble &Toulouse, France

carlo.rizzo@lncmi.cnrs.fr

Magnetic fields : a probe of matter properties

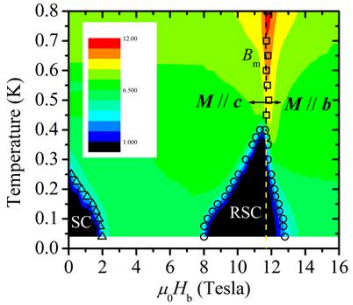

Correlated fermions, superconductivity

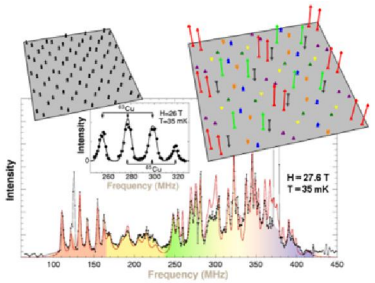

Quantum magnetism

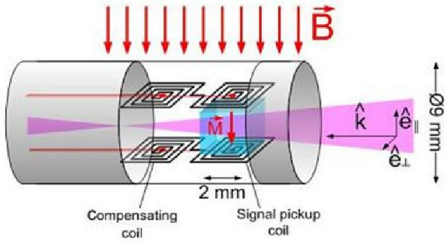

Magneto-optics

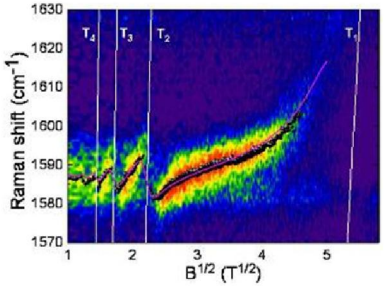

Semiconductors
Graphene

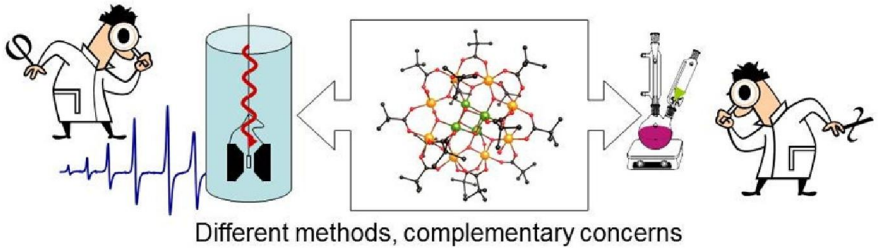

Chemistry

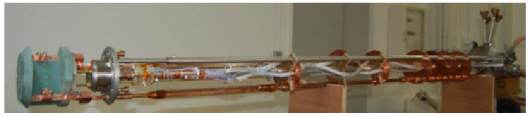

Applied superconductivity

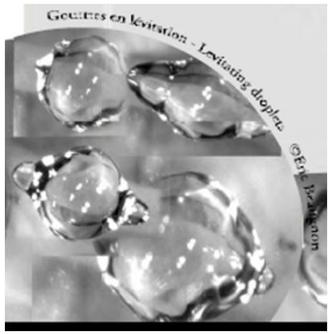

Magnetoscience levitation, elaboration under magnetic field

The European Magnetic Field Laboratory (EMFL)

HLD Dresden

Germany

HFML Nijmegen

Netherlands

EMFL

LNCMI Toulouse

France

LNCMI Grenoble

External members : United kingdom,

Potential external members : Poland, Czech republic, Estonia, Italy …

Figure 4. Three-wave mixing describes an interaction between three electromagnetic waves. These effects are not allowed in a vacuum.

Vacuum magneto-optics

see the review

R. Battesti, C. Rizzo, *Magnetic and electric properties of a quantum vacuum*, Rep. Prog. Phys. 76 (2013) 016401

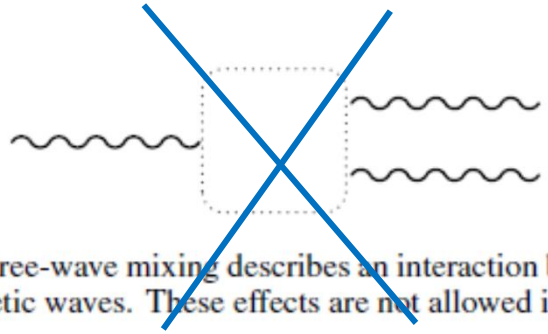

Figure 4. Three-wave mixing describes an interaction between three electromagnetic waves. These effects are not allowed in a vacuum.

Vacuum magneto-optics

see the review

R. Battesti, C. Rizzo, *Magnetic and electric properties of a quantum vacuum*, Rep. Prog. Phys. 76 (2013) 016401

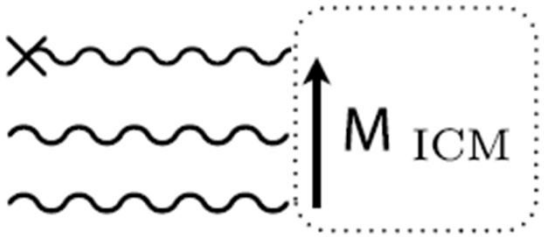

Figure 15. Inverse magneto-electric effects. Optical rectification is induced by the presence of an external magnetic or electric field. Here the interaction between two photons of the electromagnetic wave and a photon of the static magnetic field gives rise to a magnetization M. This effect is known as the ICME if the static magnetic field is perpendicular to the direction of light propagation.

Inverse effects

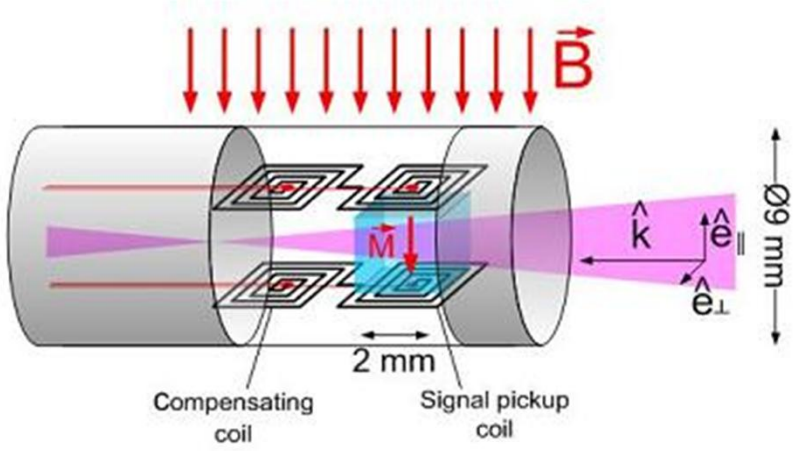

See :
Observation of the inverse Cotton-Mouton effect, A. Ben-Amar Baranga, R. Battesti, M. Fouché, C. Rizzo and G. L. J. A. Rikken, EPL **94**, 44005 (2011)
Effect in a TGG crystal

Fabry-Perot cavity

Projet	L_c (m)	F	τ (μs)	$\Delta\nu$ (Hz)	Q ($\times 10^{11}$)
REMPE	4×10^{-3}	1 900 000	8	19 400	0,2
VIRGO	3 000	50	160	1 000	2, 8
LIGO	4 000	230	980	160	17
PVLAS	3,3	770 000	2 700	59	48
BMV	2,27	481 000	1 160	137	21

[PVLAS] F. Della Valle *et al., Opt. Express* **22**, 11570 (2014)

[VIRGO] The Virgo Collaboration, *Appl. Opt.* **46**, 3466 (2007)

[LIGO] M. Rakhmanov *et al., Class. and Quantum Grav.* **21**, S487 (2004)

[REMPE] G. Rempe *et al., Opt. Lett.* **17**, 363 (1992)

The magnetic field

$$\Psi = \frac{\pi}{\lambda} k_{\mathrm{CM}} B^2 L_{\mathrm{B}} \left(\frac{2F}{\pi} \right)$$

- **Generation of a transverse magnetic field :** the X-coil coil

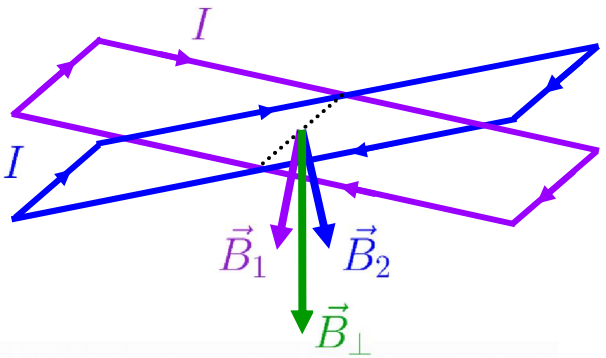

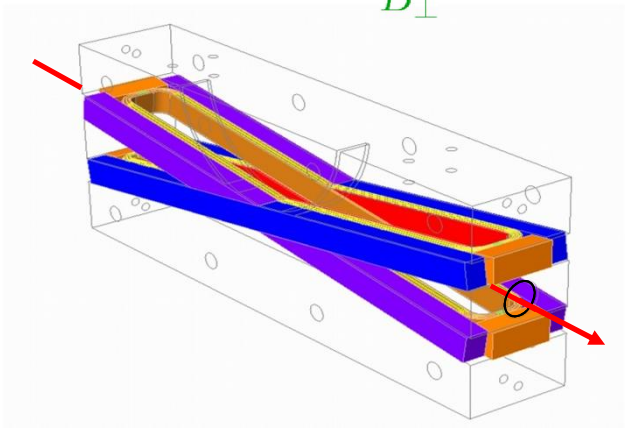

Laser beam

banc de condensateurs

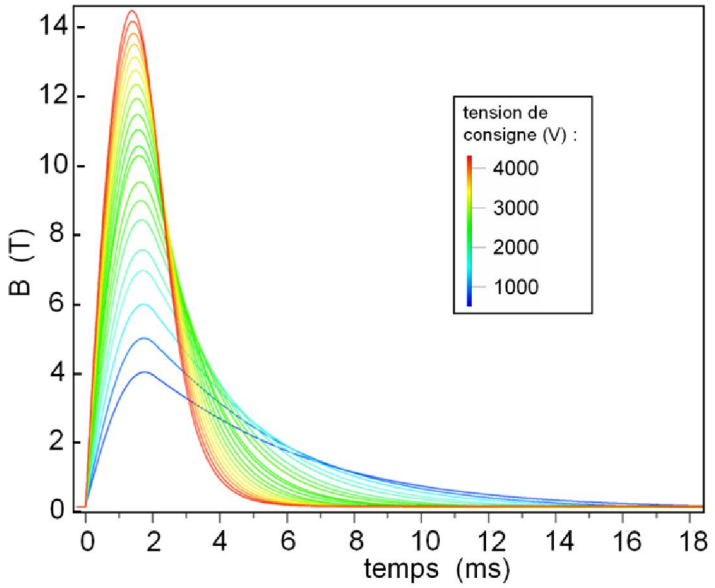

- maximum field : $B_{\mathrm{max}} = 14$ T

↳ Magnet developed at LNCMI

Experimental setup in the cleanroom at LNCMI Toulouse

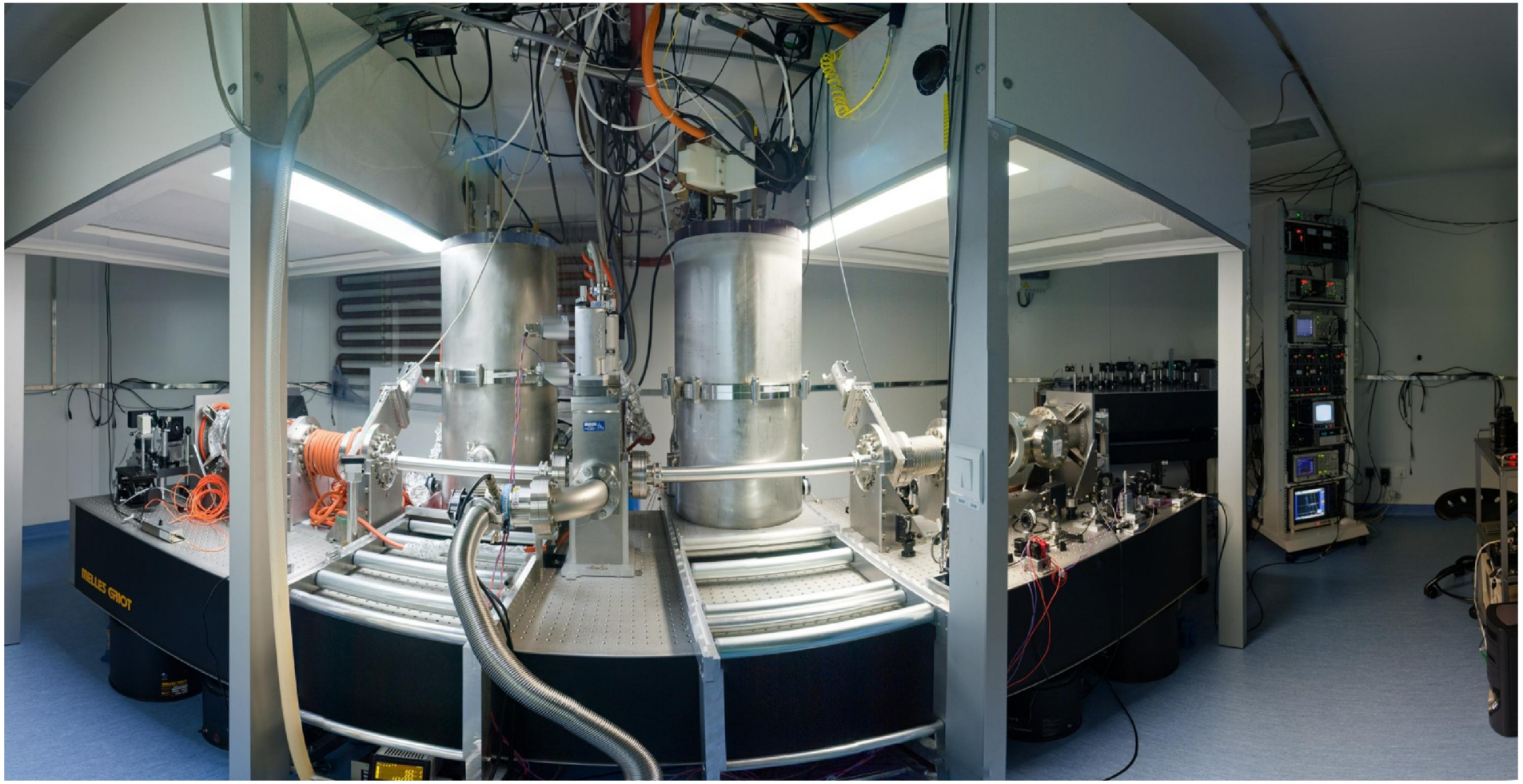

Mirrors are very sensitive to pollution (mirror losses 2×10^{-6})

POINTLIKE PARTICLES of charge Q and magnetic moment $\boldsymbol{\mu} = \mu \mathbf{e}_z$

$$\mathbf{E} = \frac{Q}{4\pi\epsilon_0 r^2}\mathbf{e}_r,$$

$$\mathbf{B} = \frac{\mu_0\mu}{4\pi r^3}\left[3\left(\mathbf{e}_z.\mathbf{e}_r\right)\mathbf{e}_r - \mathbf{e}_z\right] = \frac{\mu_0\mu}{4\pi r^3}\left(3\cos\theta\mathbf{e}_r - \mathbf{e}_z\right)$$

For a proton, $Q = 1.6 \times 10^{-19}\,\mathrm{C}$ and $\mu = 1.41\times10^{-26}\,\mathrm{J.T^{-1}}$

$$\begin{aligned}
\mathbf{P} &= c_{0,1}\sqrt{\epsilon_0\mu_0}\frac{\mu}{4\pi r^3}\left(3\cos\theta\mathbf{e}_r - \mathbf{e}_z\right) \\
&+ c_{2,0}\epsilon_0\mathbf{E}\frac{Q^2}{4\pi^2\epsilon_0 r^4}\left[1 - \left(\frac{\mu}{cQr}\right)^2\left(1+3\cos^2\theta\right)\right] \\
&+ c_{0,2}\epsilon_0 E\frac{\mu_0\mu^2\cos\theta}{4\pi^2 r^6}\left(3\cos\theta\mathbf{e}_r - \mathbf{e}_z\right) \\
&+ c_{1,1}\epsilon_0\mathbf{E}\sqrt{\frac{\mu_0}{\epsilon_0}}\frac{Q\mu\cos\theta}{4\pi^2 r^5} \\
&+ c_{1,1}\epsilon_0 E\sqrt{\frac{\epsilon_0}{\mu_0}}\frac{Q\mu_0\mu}{(4\pi)^2\epsilon_0 r^5}\left[1 - \left(\frac{\mu}{cQr}\right)^2\left(1+3\cos^2\theta\right)\right] \\
&\quad \left(3\cos\theta\mathbf{e}_r - \mathbf{e}_z\right)
\end{aligned}$$

$$\begin{aligned}
\mathbf{M} &= c_{0,1}\sqrt{\frac{\epsilon_0}{\mu_0}}\frac{Q}{4\pi\epsilon_0 r^2}\mathbf{e}_r \\
&- c_{2,0}\frac{\mathbf{B}}{\mu_0}\frac{Q^2}{4\pi^2\epsilon_0 r^4}\left[1 - \left(\frac{\mu}{cQr}\right)^2\left(1+3\cos^2\theta\right)\right] \\
&+ c_{0,2}\frac{B(\theta=0)}{\mu_0}\frac{Q^2\cos\theta}{8\pi^2\epsilon_0 r^4}\mathbf{e}_r \\
&- c_{1,1}\frac{\mathbf{B}}{\mu_0}\sqrt{\frac{\mu_0}{\epsilon_0}}\frac{Q\mu\cos\theta}{4\pi^2 r^5} \\
&+ c_{1,1}\frac{B(\theta=0)}{\mu_0}\sqrt{\frac{\epsilon_0}{\mu_0}}\frac{Q^3}{32\pi^2\epsilon_0^2\mu r^3} \\
&\quad \left[1 - \left(\frac{\mu}{cQr}\right)^2\left(1+3\cos^2\theta\right)\right]\mathbf{e}_r,
\end{aligned}$$

with $B(\theta=0) = \mu_0\mu/2\pi r^3$

Ground state values of electron g factor

State/Atom	δg_{exp}	δg_{th}	δg_{at}	δg_{QED}
$1S$ H	-35.459(26)[a]	-35.451(1)[b]	-35.5014[b]	2319.354(1)[b]
$1S$ He^{1+}	-141.9(60)[c]	-141.897(1)[b]	-142.0112[b]	2319.418(1)[b]
$1S$ $^{28}Si^{13+}$	-6970.3456(10)[d]	-6970.346491(1652)	-6976.202098(49)[e]	2325.159970(1651)[e]
$2S$ Li	-18.3(7)[f]	-14.06[g]	-14.06[g]	2319.304
$3S$ Na	-23.3(7)[f]	-20.25[g]	-20.25[g]	2319.304
$4S$ K	-25.09(24)[f]	-20.68[g]	-20.68[g]	2319.304
$5S$ Rb	11.83(20)[f]	25[h]	23[h]	2321.15[h]
$6S$ Cs	221.02(20)[f]	257	255[i]	2323.71[h]; 2319.59[j]
$7S$ Fr	2651(90)[k]	3315	3314[i]	2320.72[j]

g-factors for ground $^2S_{1/2}$ states of hydrogen, hydrogen-like $^4He^{1+}$ and Si^{13+} ions, and alkali atoms. In column 2 and 3, $\delta g_{th} = g_{th} - g_e$ and $\delta g_{exp} = g_{exp} - g_e$ report, respectively, few theoretical predictions and all the experimental data for the deviations from the g_e free electron CODATA value (Mohr et al., 2012). In column 4 $\delta g_{at} = g_{at} - 2$ represents the theoretical atomic/relativistic deviations from the Dirac value. $\delta g_{QED} = g_{QED} - 2$ of column 5 is theoretical QED contribution, including the recoil term. All values have to be multiplied by 1×10^{-6}. Refs.: [a] Tiedeman and Robinson (1977); [b] Beier (2000); [c] Jonhson and Robinson (1980); [d] Sturm et al. (2013); [e] Sturm et al. (2011); [f] Arimondo et al. (1977); [g] Marketos (1993); [h] Labzowsky et al. (1999); [i] Gossel et al. (2013); [j] Goidenko et al. (2003); [k] Ekström et al. (1986). The δg_{QED} corrections for Li, Na and K were reported byMarketos (1993) as equal to the those of the free-electron, and those value are in our Table. For Cs and Fr the δg_{th} values are obtained by us summing up the entries in columns 4 and 5, and for Cs the average δg_{QED} prediction was used.

What about excited states ?

Rubidium

Alkali metal

atomic number	37
Standard atomic weight	85.4678(3)
Electron configuration	[Kr] 5s1
Melting point	312.45 K (39.30 °C)
Boiling point	961 K (688 °C)

Typical cell containing solid rubidium in equilibrium with its vapour

NMR accurate magnetic field measurement

A spin ½ particle, like a proton, if a magnetic field is present, undergoes an energy splitting proportional to the field strength

γ_P = 42.5774806(10) MHz/T

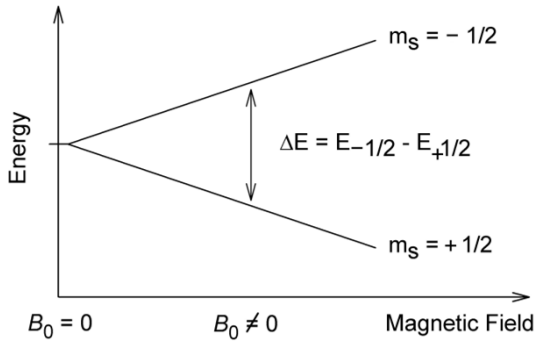

RF or MW electromagnetic probe can be resonant with the transition between the two levels

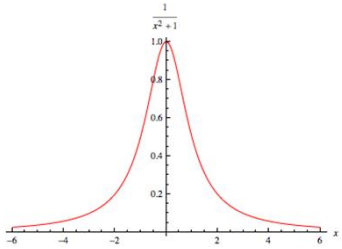

Electronic frequency counting

Magnetic field value

Commercial NMR teslameters are based on this frequency-field conversion. Standard precision is 0.1 ppm for a highly homogeneous field. Absolute accuracy 5 ppm

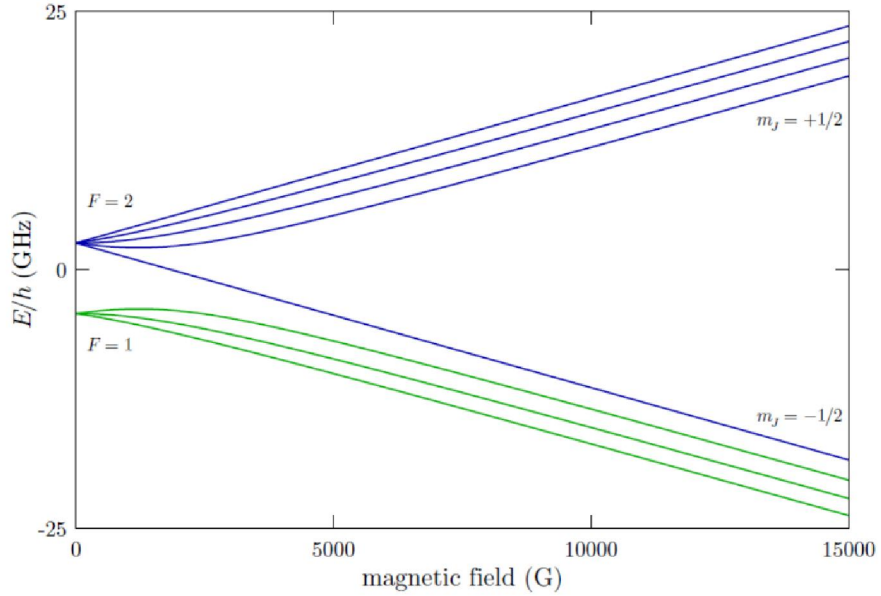

^{87}Rb ground state in a magnetic field

Analytical Breit-Rabi formula

$$E_{|J=1/2\, m_J\, I\, m_I\rangle} = -\frac{\Delta E_{\rm hfs}}{2(2I+1)} + g_I\,\mu_{\rm B}\,m\,B \pm \frac{\Delta E_{\rm hfs}}{2}\left(1 + \frac{4mx}{2I+1} + x^2\right)^{1/2}$$

with $x = \dfrac{(g_J - g_I)\mu_{\rm B}\,B}{\Delta E_{\rm hfs}}$

$m = m_I \pm m_J$

$\Delta E_{\rm hfs}/h$ = ½ x 3.41734130545214 5(45) GHz

g_j^g = 2.002331113(20)

g_i^g = -0.0009951414(10)

Landé g-factors

μ_B/h = 13.99624604(35) GHz/T

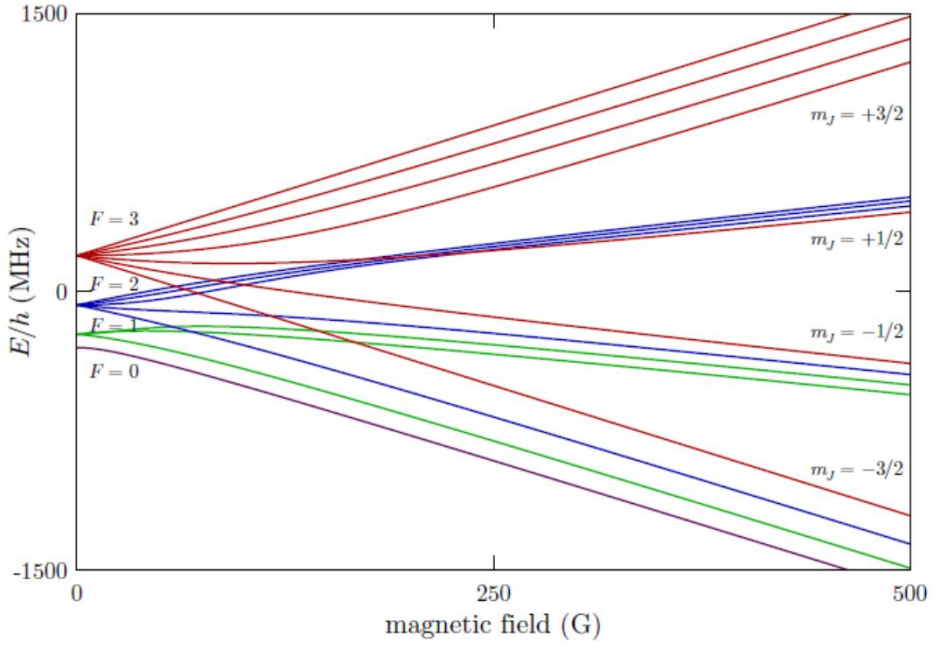

^{87}Rb excited level
in a magnetic field

No analytical formula exists, thus one has to calculate numerically the energy of every level using standard quantum mechanics

$\Delta E_{hfs}/h$ = ½ x 84.7185(20) MHz

g_j^e = 1.3362(13) measured
g_j^e = 1.33411 theoretical

QED correction expected at 10^{-5}-10^{-6} level

Arimondo et al., RMP, 1977
Flaumbaum et al.,PRA, 2013
Steck, Rubidium 87 D Line Data, 2010

Towards an accurate optical magnetometer designed to be used in high magnetic field coils.

20 mm diameter fiber coupled probe based on a mini cell

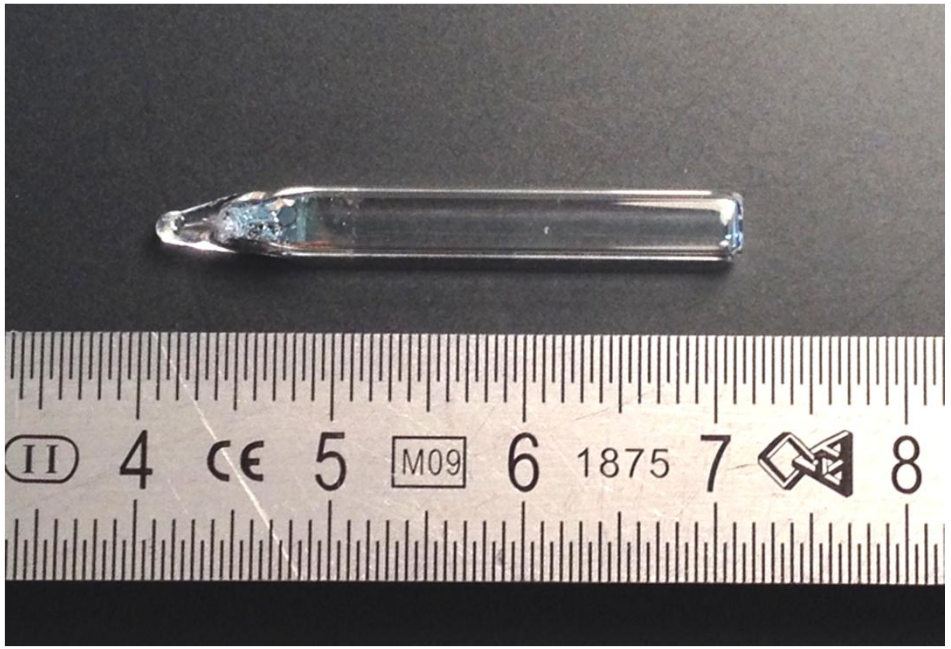

3 mm x 3 mm mini-cell

Observation of transmission and/or fluorescence from the minicell

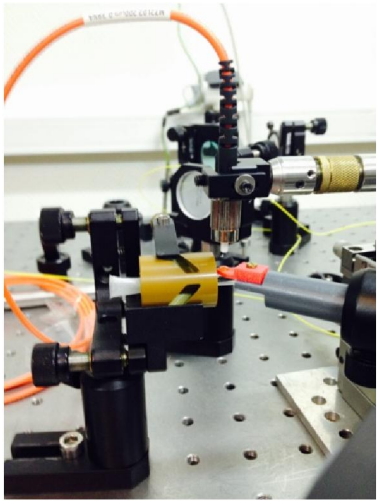

absorption of a reference cell

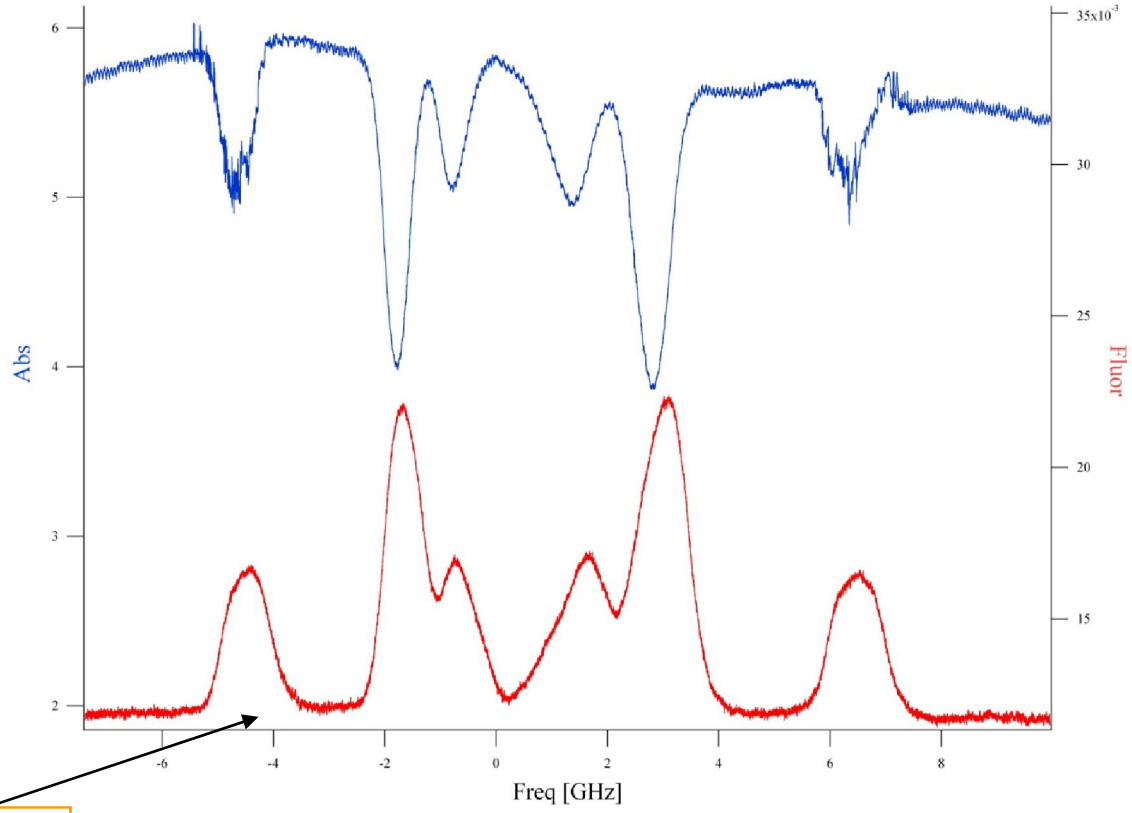

First results with a
test set up at B=0 T

4 nW from
2000 atoms
in a volume of
200 μm diameter

fluorescence of the mini-cell